21. Sigmundsson T, Suckling J, Maier M, Williams SCR, Bullmore ET, Greenwood KE, Fukuda R, Ron MA, Toone BK (2001) Structural abnormalities in frontal, temporal, and limbic regions and interconnecting white matter tracts in schizophrenic patients with prominent negative symptoms. Am J Psychiatry 158:234–243
22. Ture U, Yasargil DC, Al-Mefty O, Yasargil MG (1999) Topographic anatomy of the insular region. J Neurosurg 90:720–733
23. Varnavas GG, Grand W (1999) The insular cortex: morphological and vascular anatomic characteristics. Neurosurgery 44:127–136 (discussion 136–138)
24. Wilke M, Kaufman C, Grabner A, Putz B, Wetter TC, Auer DP (2001) Gray matter-changes and correlates of disease severity in schizophrenia: a statistical parametric mapping study. NeuroImage 13:814–824
25. Wright IC, Ellison ZR, Sharma T, Friston KJ, Murray RM, McGuire PK (1999) Mapping of grey matter changes in schizophrenia. Schizophr Res 35:1–14
26. Yamada M, Hirao K, Namiki C, Hanakawa T, Fukuyama H, Hayashi T, Murai T (2007) Social cognition and frontal lobe pathology in schizophrenia: A voxel-based morphometric study. NeuroImage 35:292–298
27. Yamasaki S, Yamasue H, Abe O, Yamada H, Iwanami A, Hirayasu Y, Nakamura M, Furukawa SI, Rogers MA, Tanno Y, Aoki S, Kato N, Kasai K (2007) Reduced planum temporale volume and delusional behaviour in patients with schizophrenia. Eur Arch Psychiatry Clin Neurosci (in press)

Temporal Change in Human Nicotinic Acetylcholine Receptor After Smoking Cessation: 5IA SPECT Study

Marcelo Mamede[1], Koichi Ishizu[1], Masashi Ueda[2], Takahiro Mukai[1], Yasuhiko Iida[2], Hidekazu Kawashima[2], Hidenao Fukuyama[3], Kaori Togashi[1], and Hideo Saji[2]

[1]Department of Diagnostic Imaging and Nuclear Medicine, Graduate School of Medicine, Kyoto University, Kyoto, Japan; [2]Department of Patho-Functional Bioanalysis, Graduate School of Pharmaceutical Science, Kyoto University, Kyoto, Japan; and [3]Brain Function Imaging Division, Human Brain Research Center, Graduate School of Medicine, Kyoto University, Kyoto, Japan

Nicotinic acetylcholine receptors (nAChRs) are of great interest because they are implicated in various brain functions. They also are thought to play an important role in nicotine addiction of smokers. Chronic (−)-nicotine, a nAChR agonist, treatment in mice and rats elicits a dose-dependent increase in nAChRs in the brain. Upregulation of nAChRs in postmortem human brains of smokers has also been reported. However, changes in nAChRs after cigarette smoking cessation in humans are poorly understood. The aim of this study was to detect the dynamic changes of nAChRs after smoking and smoking cessation in the brains of living subjects. **Methods:** We performed 5-^{123}I-iodo-A-85380 (^{123}I-5IA) SPECT on nonsmokers and smokers (n = 16) who had quit smoking for 4 h, 10 d, and 21 d and calculated and compared distribution volumes (Vt) of ^{123}I-5IA. **Results:** The binding potential of nAChRs (Vt of ^{123}I-5IA) in the brains of smokers decreased by 33.5% ± 10.5% after 4 h of smoking cessation, increased by 25.7% ± 9.2% after 10 d of smoking cessation, and decreased to the level of nonsmokers after 21 d of smoking cessation. **Conclusion:** Because the upregulation of the nAChRs of the smokers after chronic exposure of the nicotine was downregulated to the nonsmokers' level by around 21 d after smoking cessation, the upregulation is a temporary effect. The decrease in nicotinic receptors to nonsmoker levels may be the breaking point during the nicotine withdrawal period.

Key Words: ^{123}I-5IA; SPECT; nicotinic acetylcholine receptors; human brain; smoking withdrawal; quantitative measurement

J Nucl Med 2007; 48:1829–1835
DOI: 10.2967/jnumed.107.043471

Nicotinic acetylcholine receptors (nAChRs) are a family of ligand-gated ion channels that regulate neurotransmission in the central and peripheral nervous systems. These receptors are of great interest because they are implicated in various brain functions, including cognition and memory (*1,2*) and in nicotine-induced neuroprotective (*3*) and analgesic effects (*4*). In addition, these receptors are thought to play an important role in nicotine addiction (*5*).

Chronic treatment with agonists for most neurotransmitter receptor systems results in a decrease in receptor number. However, it has been demonstrated that chronic treatment of mice (*6*) and rats (*7*) with (−)-nicotine, an nAChR agonist, elicits a dose-dependent increase in nAChRs. This upregulation is not permanent, returning to control levels within 7–10 d in mice (*6*) and 15–20 d in rats (*8,9*) after cessation of (−)-nicotine treatment. Previous efforts to demonstrate nAChR upregulation in the human brain have also been reported primarily in in vitro binding assays (*10,11*). Kassiou et al. reported the upregulation of nAChRs with chronic (−)-nicotine treatment in the brain of a live baboon (*12*). More recently, Staley et al. described the upregulation of nAChRs in human brains after early abstinence of tobacco smoking using 5-^{123}I-iodo-A-85380 (^{123}I-5IA) and SPECT images (*13*). However, changes in nAChRs in humans after cessation of smoking are poorly understood. Breese et al. studied the levels of ^{3}H-nicotine binding in humans postmortem for changes in nicotinic receptor levels and reported that the nAChR levels in smokers who had stopped smoking at least 2 mo before their death were similar to those in nonsmokers (*14*); the effects of shorter-term smoking cessation are unknown.

^{123}I-5IA is a nAChR imaging probe that has extremely high selectivity and specificity for the α4β2 subunit of nAChRs in rodent (inhibition constant = 0.37 nM) (*15*) and primate brain in vivo (*16*), with relatively low acute toxicity (effective dose equivalent = 30 μSv/MBq) (*17,18*). Moreover, we have developed the methodology for the quantification of nAChRs in human brain using ^{123}I-5IA and SPECT (*19*).

The aim of the present study was to detect the dynamic changes of nAChRs in living human brain after smoking and smoking cessation. We performed ^{123}I-5IA SPECT on nonsmokers and smokers who had quit smoking for 4 h, 10 d, and

Received May 9, 2007; revision accepted Jul. 30, 2007.
For correspondence or reprints contact: Koichi Ishizu, MD, PhD, Department of Diagnostic Imaging and Nuclear Medicine, Graduate School of Medicine, Kyoto University, Sakyo, 606-8507, Kyoto, Japan.
E-mail: ishizu@kuhp.kyoto-u.ac.jp

21 d and compared the distribution volumes (*Vt*) of ^{123}I-5IA of each group and with nonsmokers. To our knowledge, this is the first in vivo imaging study of nAChR upregulation and recovery in response to short-term smoking cessation in living subjects.

MATERIALS AND METHODS

Volunteers

Six male nonsmokers (23 ± 6 y) and 10 healthy male smokers (28 ± 4 y) were included in this study. Five smokers in the 4-h group were also included in either the 10-d or the 21-d group. In total, 21 ^{123}I-5IA SPECT studies were acquired (Table 1). None of the subjects had a history of neurologic or psychiatric illness or the use of psychotropic or sleep-inducing drugs. The nonsmokers had no history of smoking tobacco.

For the smoking withdrawal studies, the smokers were divided in 3 groups: 5 subjects (age, 28 ± 4 y) for 4-h withdrawal, 5 subjects (age, 27 ± 6 y) for 10-d withdrawal, and 5 subjects (age, 28 ± 3 y) for 21 d of smoking withdrawal. The 4 groups were age-matched.

All subjects gave written informed consent to participate in this study in compliance with the regulations of the Joint Committee on Clinical Investigation of the Kyoto University Hospital.

Radiolabeling

Radiolabeling of the ^{123}I-5IA followed the methods we reported previously (*19*). To a sodium ^{123}I-iodide solution (1,110 MBq) (Nihon Medi-Physics), 100 μg of (*S*)-5-(tri-*n*-butylstannyl)-3-([1-*t*-butoxycarbonyl-2(*S*)-azetidinyl]methoxy)pyridine, 1.5% acetic acid, 3 mol/L HCl, and 5% H_2O_2 solution were added, and the mixture was stirred at 75°C for 15 min. Concentrated HCl was then added, and the resulting solution was stirred for another 10 min at 75°C. The mixture was made basic with NaOH and extracted with ethyl acetate, and the organic layer was evaporated. The residue was purified by reverse-phase high-performance liquid chromatography ([HPLC] Cosmosil 5C18-AR-300, 10 × 250 mm; Nacalai Tesque; 10 mmol/L ammonium acetate/methanol/triethylamine = 752:750:2; 1.5 mL/min; retention time for 5IA was 40 min). After evaporation of the HPLC eluent, the residue was dissolved in 0.9% saline and filtered through a 0.2-μm filter into a sterile vial. Radiochemical purity was >98%, and radiochemical yields were ~42%. The specific activity determined from the ultraviolet absorbance at 254 nm was >169 GBq/μmol (the detection limit for this method).

SPECT

All subjects underwent a set of 5 SPECT dynamic scans (a 120-min scan, followed by 4 sets of 20-min scans). All SPECT dynamic scans were acquired with a triple-head rotating γ-camera system (PRISM 3000; Picker International) equipped with low-energy, high-resolution, fanbeam collimators. Data acquisition and image reconstruction were performed as in our previous study (*19*). The data acquisition was alternately performed over 120 min after intravenous injection of ^{123}I-5IA, followed by 4 sets of 20-min scans (at 3, 4, 5, and 6 h after the injection). SPECT images were reconstructed using a filtered backprojection algorithm with a ramp filter. Attenuation correction was performed using ellipses outer line approximation and Chang's method (coefficient of 0.06/cm), which assumes that the attenuation process is homogeneous throughout the brain and can be described by an exponential function. Scatter correction was not applied.

A dose of ~150 MBq of ^{123}I-5IA was administered intravenously over a period of 1 min at a constant rate with an infusion pump, and the SPECT scan was started at the same time as the injection. Arterial blood sampling and metabolite correction were also performed to estimate the arterial input function of the ^{123}I-5IA for each volunteer by the same method as that used in our earlier study (*19*).

TABLE 1
Study Groups

Nonsmokers	Smokers: period of smoking cessation		
	4 h	10 d	21 d
Subject 1	Subject 7	Subject 7	Subject 9
Subject 2	Subject 8	Subject 8	Subject 10
Subject 3	Subject 9	Subject 12	Subject 11
Subject 4	Subject 10	Subject 13	Subject 15
Subject 5	Subject 11	Subject 14	Subject 16
Subject 6			

Arterial Input Function

Twenty-five arterial blood samples were obtained at the same time points as described previously (*19*). From each sample, 100 μL of plasma were removed and the radioactivity was measured in an automatic well-type γ-counter (Cobra 2; Packard Instruments). Sixteen samples were analyzed by thin-layer chromatography (TLC) (10% ammonium acetate and methanol [1:1], LK6DF Silica Gel, 60 Å; Whatman) for metabolite determination (R_f = 0.55 for ^{123}I-5IA) (*19*). The measured unmetabolized fractions were fitted with a dual exponential curve, and the input function was calculated as all plasma sample counts were corrected for metabolites using the fitted curve.

Data Analysis

Reconstructed SPECT images were automatically coregistered using a coregistration algorism of statistical parametric mapping, SPM99 (Welcome Department of Cognitive Neurology, London, U.K.), to minimize positional error caused by head movement during the scans. Multiple circular regions of interest (ROIs) (21 pixels per circle) were manually drawn in each brain region (basal ganglia, thalamus, brain stem, cerebellum, frontal, parietal, temporal, and occipital cortices) on both sides. ROI data were further decay-corrected. SPECT data were calibrated to the well counter used to measure the injected activity. Time–activity curves were generated from the ROIs and the dynamic image datasets.

Kinetic analysis of the ^{123}I-5IA was performed using a 2-compartment model including K_1 and k_2 rate constants and a curve-fitting method following our previous study (*19*). *Vt* values of the ^{123}I-5IA were calculated and used as a quantitative index correlated with the regional binding potential of the nAChRs. The *Vt* values were further evaluated in terms of interval change after the smoking withdrawal.

Statistical Analysis

All data are expressed as the mean ± SD. The *Vt* values obtained from the different regions in the brain were analyzed by 1-way ANOVA with the Bonferroni protected least significant difference test. The interval changes of the ^{123}I-5IA *Vt* were analyzed between the 3 phases after the smoking withdrawal using the Tukey–Kramer multiple comparison test. All tests were 2-sided, and probability values of $P < 0.05$ were considered significant.

RESULTS

As in our previous study (*19*), the characteristics of the arterial input functions for all volunteers (nonsmokers and smokers) were similar. The peak plasma activity occurred between 70 and 80 s after injection in all subjects and decreased rapidly to 6.5%–9.0% of the peak level in 10 min. Analysis of the unmetabolized compound by TLC demonstrated a high parent fraction of ^{123}I-5IA in the plasma (87.7% ± 6.3%) in the first minute. ^{123}I-5IA was rapidly metabolized, and the unchanged fraction represented 50.9% ± 8.8% and 32.4% ± 12.6% of total plasma activity at 20 and 60 min, respectively.

Figure 1 shows the representative standardized time–activity curve of ^{123}I-5IA in the frontal cortex. The concentrations of radioactivity were slightly higher in the nonsmokers and in the 4-h smoking-cessation group followed by the 10-d and 21-d smoking-cessation groups. The peaks of radioactivity occurred ~50 min after injection of ^{123}I-5IA for nonsmokers and for the 4-h and 21-d smoking-cessation groups, whereas it was at ~70 min for the 10-d smoking-cessation group. A differential dissociation of ^{123}I-5IA from the binding sites was noted in the brain. The 4-h smoking-cessation group showed a faster dissociation compared with that of the nonsmokers. However, the 10-d and 21-d smoking-cessation groups showed a slower dissociation than that of the nonsmokers (more pronounced in the 21-d group). These findings reflected a temporal change of the nAChRs in the human brain.

Packs per day and pack years of cigarette smoking before cessation were similar for the different groups of smokers (Table 2). Only 2 subjects (subjects 7 and 11) had detectable amounts of nicotine in their plasma after 4-h smoking cessation (Table 2).

To validate the *Vt* values of the nonsmokers as a baseline group, we compared (*t* test) our current data (nonsmokers) with our published data (*19*). No significant difference was observed between these groups. Similar findings were also seen for K_1 and k_2. Therefore, we used the *Vt* values from nonsmokers as a reference for further comparisons with groups of smokers at several smoking-cessation intervals.

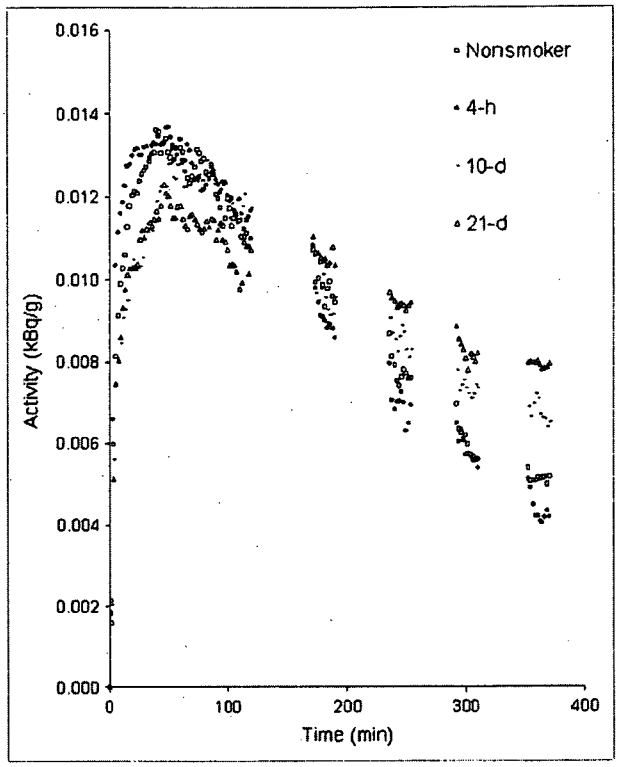

FIGURE 1. Representative standardized time–activity curves of ^{123}I-5IA in frontal cortex from a nonsmoker and smokers.

Table 3 describes the *Vt* values of different groups of volunteers (nonsmokers and smokers). There was a significant difference among those groups (ANOVA; $P < 0.001$). Individualized comparisons between 2 groups of volunteers were also performed. After 4 h of smoking cessation, the *Vt* values in all brain regions decreased significantly compared with those of the nonsmoker group ($P < 0.05$, except for frontal, parietal, and occipital cortices). On the other hand, after 10 d of smoking cessation, the *Vt* values were significantly higher than those of nonsmokers ($P < 0.05$, except for basal ganglia and thalamus). Then, after 21 d of smoking cessation, the *Vt* values decreased significantly compared

TABLE 2
Characteristics of Volunteers and Plasma Concentration of Nicotine and Cotinine

Group	Age (y ± SD)	Packs/d	Pack years	Plasma concentration (ng/mL)	
				Nicotine	Cotinine
Nonsmokers	24 ± 6	—	—	ND	ND
Smokers					
4-h withdrawal	28 ± 4	0.8 ± 0.3	6.1 ± 4.3	7.6, 8.9*	282 ± 189
10-d withdrawal	27 ± 6	0.8 ± 0.2	6.3 ± 3.9	ND	ND
21-d withdrawal	28 ± 3	0.8 ± 0.3	6.3 ± 4.5	ND	ND

*Results from only 2 subjects (3 other subjects had nondetectable values).

Packs/d = number of packs smoked per day; Pack years = number of packs per day while smoking multiplied by number of years smoked; ND = not detected (detection limits for nicotine and cotinine were 5.0 and 100 ng/mL, respectively).

Values are expressed in mean ± SD.

TABLE 3

^{123}I-5IA V_t Estimates for 2-Compartment, 2-Parameter Model for Various Brain Regions from Nonsmokers and Smokers After Withdrawal of Cigarette Smoking

Subject	Frontal	Parietal	Temporal	Occipital	BG	Thalamus	BS	Cerebellum
Nonsmokers								
1	14.3	13.2	13.2	11.2	15.8	30.1	22.9	15.6
2	20.3	18.9	19.7	16.2	24.2	43.2	35.5	20.5
3	14.1	13.0	13.8	11.2	16.0	28.4	22.3	14.9
4	14.4	14.4	14.6	11.7	17.2	31.1	25.3	18.4
5	11.3	10.7	10.7	9.5	12.9	19.3	17.7	14.4
6	13.2	12.2	12.2	11.1	13.5	20.9	18.7	13.7
Mean	14.6	13.7	14.0	11.8	16.6	28.8	23.7	16.3
SD	3.0	2.8	3.1	2.3	4.0	8.6	6.4	2.7
Smokers								
4-h withdrawal								
7	6.1	6.3	6.4	5.9	6.5	7.0	7.0	5.9
8	12.6	13.0	12.2	11.4	12.8	16.1	14.0	11.3
9	14.9	14.0	13.7	12.5	15.0	21.3	19.4	14.4
10	8.7	8.4	8.6	7.6	10.0	13.5	12.2	8.8
11	10.2	10.4	10.2	9.0	11.2	12.9	12.3	10.0
Mean	10.5	10.4	10.2	9.3	11.1	14.1	13.0	10.1
SD	3.4	3.2	2.9	2.7	3.2	5.2	4.4	3.1
10-d withdrawal								
7	19.7	19.3	19.2	17.5	21.0	31.1	29.4	20.9
8	19.1	18.7	17.4	16.4	19.4	28.7	25.3	20.7
12	18.0	17.6	17.4	16.1	20.2	28.9	30.3	22.4
13	16.1	16.2	16.4	15.2	18.7	28.9	29.3	20.8
14	19.2	18.1	17.8	15.8	21.5	36.5	32.8	23.9
Mean	18.4	18.0	17.6	16.2	20.2	30.8	29.4	21.7
SD	1.4	1.2	1.0	0.9	1.2	3.3	2.7	1.4
21-d withdrawal								
9	15.3	14.6	14.6	12.2	17.6	28.4	23.6	19.7
10	14.4	14.3	13.8	12.1	17.5	31.3	24.9	17.2
11	17.0	16.6	15.9	13.6	18.5	27.0	26.1	20.1
14	14.1	14.0	13.6	12.8	15.5	21.6	21.0	15.7
15	14.4	14.1	13.6	12.2	15.7	27.0	22.7	15.7
Mean	15.1	14.7	14.3	12.6	17.0	27.0	23.7	17.7
SD	1.2	1.1	1.0	0.6	1.3	3.5	2.0	2.1

BG = basal ganglia; BS = brain stem.
Reported as mean for V_t estimates from 2-compartment model. Values for V_t are in mL/g.

with those of the 10-d group ($P < 0.01$, except for thalamus), returning to the level in nonsmokers (Vt values did not show any significant difference compared with those in the nonsmokers). Figure 2 shows the percentage of reduction and increment in each group of smokers in comparison with the nonsmoker group. In the Tukey–Kramer multiple comparison test, the interval changes of the ^{123}I-5IA Vt between the 3 phases after the smoking cessation were significantly different ($P < 0.001$).

The rate constant K_1 had some fluctuations among the different groups of volunteers (nonsmokers and smokers); however, these differences were not statistically significant (ANOVA; not significant) (Fig. 3A). On the other hand, the values of the rate constant k_2 were significantly different among the groups of volunteers (ANOVA; $P < 0.01$) (Fig. 3B). This difference was due basically to the increase of k_2 in the group with 4 h of smoking cessation.

DISCUSSION

The present study described the effect of nicotine intake in tobacco smokers and smoking cessation on the high-affinity nicotinic receptors in humans using ^{123}I-5IA SPECT. To our knowledge, this is the first in vivo imaging of nAChR up-regulation and recovery in response to short-term smoking cessation in living smokers.

Previous animal studies have shown that chronic nicotine treatment induces an increase in high-affinity nicotinic receptor binding (*6–9*), and human postmortem studies have found a similar increase in ^{3}H-nicotine binding to high-affinity receptors in the postmortem cortex, cerebellum, and hippocampus of smokers compared with that in nonsmokers (*10–12*).

The mechanism by which the chronic exposure of nicotine evokes an increase in the density of the binding sites is not fully understood. Marks et al. reported that the increase in nicotinic receptor numbers in rodents is not caused by an

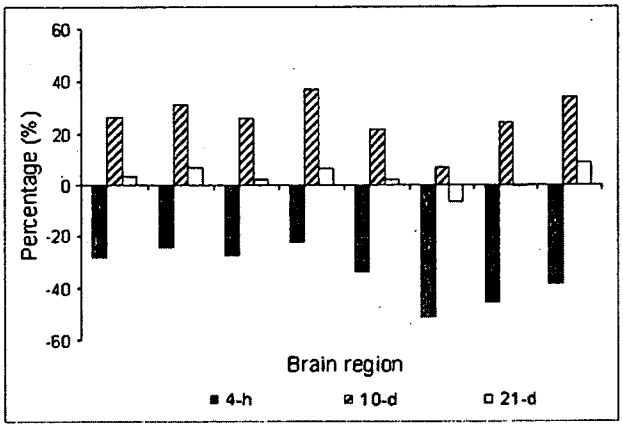

FIGURE 2. Percentage of reduction and increment of *Vt* of ^{123}I-5IA in smokers after smoking cessation compared with nonsmokers. Eight brain regions are frontal, parietal, temporal, occipital, basal ganglia, thalamus, brain stem, and cerebellum from the left, respectively.

increase in messenger RNA levels (*20*). The lack of an effect on nicotinic receptor transcription in mice suggests that nicotine-induced increases in nicotinic receptor levels are most likely related to a decrease in receptor turnover (*21*). The increase in nicotinic receptor number and the decreased rate of receptor turnover may be related to nicotinic receptor channel desensitization, which appears to reflect the conformational state of the receptor channel (*21,22*). Once the nicotinic receptor channels are desensitized and rendered inactive, additional receptors would be recruited to maintain the nicotinic response of the neuron, which results in an overall increase in nicotine binding, possibly due to a conversion of low-affinity receptors to a conformation with a high affinity for agonists (*23*).

In this study, the ^{123}I-5IA *Vt* measured at 4 h after smoking cessation was significantly lower than that in nonsmokers. The mean value of the calculated *Vt* of the smokers was ~33.5% ± 10.5% lower than that of nonsmokers and was more pronounced in the thalamus (51%) and brain stem (45%). In this group of volunteers, the plasma nicotine level 4 h after smoking cessation was detectable in only 2 subjects and was below the detection limit in the other subjects. Nicotine is highly lipophilic and demonstrated high levels of nonspecific uptake in brain (*24,25*). Rowell and Li have reported that levels of nicotine in the brain were ~3-fold higher than those in the plasma (*7*), which explains the lack of plasma nicotine measurements in 3 subjects in this group of volunteers. Because of high levels of nonspecific uptake of nicotine in the brain, nicotine or its metabolites may accumulate in nonspecific compartments in the brain (i.e., white matter) and then diffuse slowly into areas with higher levels of nAChRs, maintaining high levels of occupancy of the nAChRs. In addition, Brody et al. have shown saturation of the nicotinic receptors in human brain for up to 4 h in smokers (*26*). Thus, we would expect some level of nicotine or metabolites in the brain that would compete with ^{123}I-5IA and impair imaging of the upregulation of nAChRs. Also, we believe that some level of nicotine in the brain resulted in a high level of occupancy of the receptors, which reduced specific tracer uptake (*27*). Because of competitive binding between the radioligand and nicotine in the brain, imaging of upregulation of nAChRs in vivo requires sufficient time for nicotine clearance (>4-h smoking cessation).

After 10 d of smoking cessation, the *Vt* of ^{123}I-5IA was significantly higher than that in nonsmokers, with a 25.7% ± 9.2% increase among brain regions. The result of the increased *Vt* of the ^{123}I-5IA was in agreement with the upregulation of the nAChRs in the brains of smokers reported in postmortem human studies (*10–12*) and in animal studies (*6–9*). Staley et al. have described similar findings in human brain (*13*). The authors noted that after 6.8 ± 1.9 d of tobacco abstinence, the uptake of ^{123}I-5IA increased significantly throughout the cerebral cortex (26%~36%) in smokers (*13*). After 10 d of smoking cessation, nicotine and cotinine were not detected in the plasma. Thus, blood nicotine levels were negligible in the ^{123}I-5IA SPECT scans of smokers as well as nonsmokers.

After 21 d of smoking cessation, the *Vt* of ^{123}I-5IA was significantly lower compared with that after 10 d of smoking cessation and was not significantly different from that in the nonsmokers. Breese et al. showed that smokers who had quit at least 2 mo before death had nicotinic receptor binding levels similar to those in nonsmokers (*14*). In the present study, the interval of 21 d was thought to be the recovery time during which upregulated nAChRs return to the level of the nonsmoker. This suggests that nicotine-induced upregulation of receptor number is a temporary effect, similar to that found in rodents (*28,29*).

The upregulation of the nAChRs was similar in almost all brain regions, except the thalamus and basal ganglia, which showed a slightly different pattern. In thalamus and basal ganglia, after 10 d of smoking cessation the *Vt* was higher than that of the nonsmokers, as in the other regions, but was not significantly different. Staley et al. have shown similar findings (*13*). In addition, it has been reported in a study of mice that nicotine-induced increases in nicotinic receptor numbers do not increase to the same degree in all brain regions (*30*). Moreover, the nicotinic receptor is more abundant in the thalamus, with greater receptor heterogeneity, than in other brain regions (*19*). However, the characteristics of the acute response of neuronal nAChRs to nicotine depend on their subunit composition (*31,32*). Nicotinic receptor subtypes are affected differentially by chronic exposure to nicotine, both in cell models (*33–35*) and in vivo (*35*). Multiple factors are thought to be responsible for these differences.

This study should be interpreted in the context of several limitations. (a) The number of subjects evaluated was small, which reduced the statistical accuracy. (b) The study design used did not allow us to deal with a within-subject analysis of the whole group, as the variables were analyzed independently. (c) The smokers varied in their rate and depth of inhalation of smoke, and these interindividual

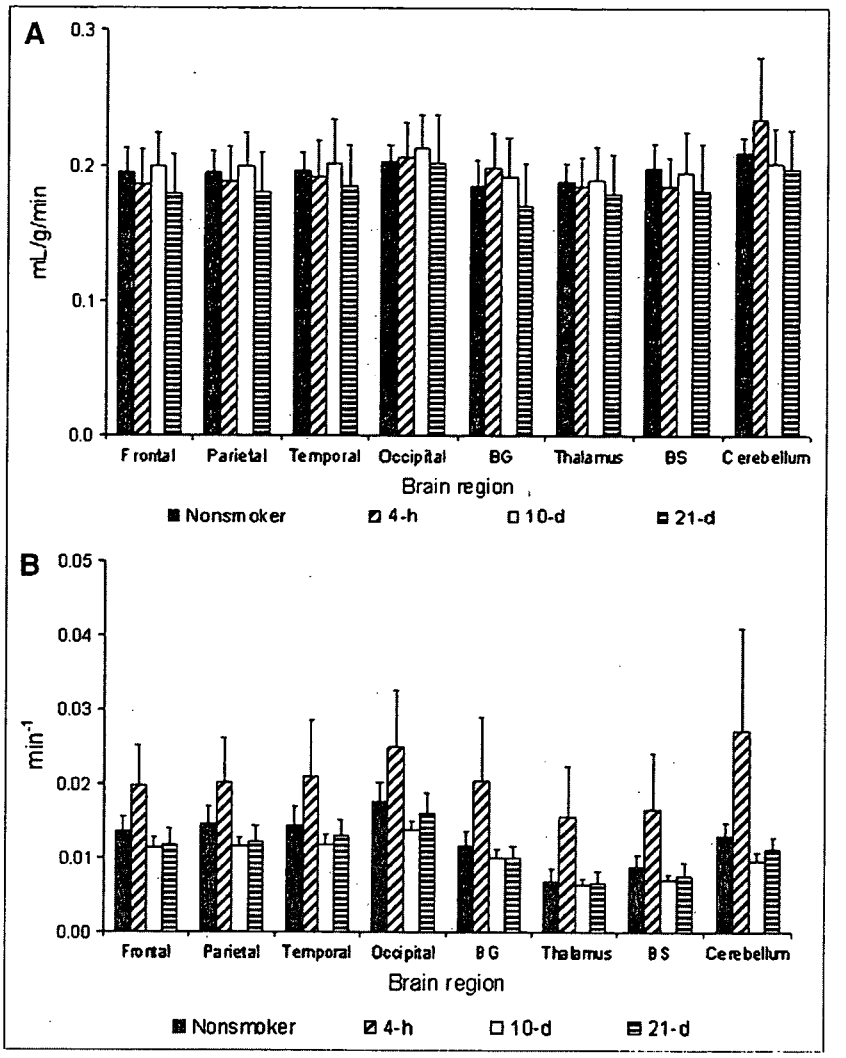

FIGURE 3. Temporal changes in rate constants K_1 and k_2 in nonsmokers and smokers after smoking cessation. (A) Rate constant K_1 (mL/g/min). (B) Rate constant k_2 (min^{-1}). BG = basal ganglia; BS = brain stem.

differences could have affected our measurements. (d) The detection limit of the plasma nicotine measurements was not enough to evaluate all blood samples. Thus, we were not able to correlate the plasma nicotine/cotinine levels with *Vt*. (e) We have not coregistered SPECT images with MRI, which would have been the most appropriate method for placement of ROIs. (f) We have not evaluated the smoker's behavior during the smoking-cessation period. We believe that the nicotine binding and desensitization of the nAChRs in the brain alleviate the cigarette craving and that craving will be the worst during the first 10 d of cessation due to the upregulation of nAChRs. The craving process should minimize after 21 d, as we observe similar levels of occupancy as nonsmokers at that time. However, we cannot exclude the possibility of other nAChR subtypes being involved in the process of tobacco dependence.

CONCLUSION

We have described the in vivo imaging of nAChR upregulation and recovery in response to short-term smoking cessation in smokers using ^{123}I-5IA SPECT. Our results clearly suggest that tobacco smoking is associated with an upregulation of nicotine binding sites in the brain. The upregulation of the nAChRs of the smokers after chronic exposure to nicotine was downregulated to the level in nonsmokers after ~21 d of smoking cessation. Thus, the upregulation of receptor numbers is a temporary effect. Nicotine dependence and difficulty in smoking cessation are also interesting with regard to the findings of the ^{123}I-5IA SPECT study. The decrease in nicotinic receptors to nonsmoker levels may be the breaking point during the nicotine withdrawal period.

ACKNOWLEDGMENTS

The authors thank Dr. Masanori Ichise (Department of Radiology, Columbia University, College of Physicians and Surgeons) for his tremendous editorial support and suggestions on this project. The authors also thank Nihon Medi-Physics Co. Ltd., Japan, for providing sodium ^{123}I-iodide.

This work was supported in part by a grant from the Research for the Future Program of the Japan Society for the Promotion of Science (JSPS-RFTF97K00201); Grants-in-Aid for Scientific Research from the Ministry of Education, Science and Technology of Japan; a research grant from Longevity Sciences from the Ministry of Health and Welfare; and a grant from the Smoking Research Foundation.

REFERENCES

1. Gotti C, Fornasari D, Clementi F. Human neuronal nicotinic receptors. *Prog Neurobiol.* 1997;53:199–237.
2. Paterson D, Nordberg A. Neuronal nicotinic receptors in the human brain. *Proc Neurobiol.* 2000;61:75–111.
3. Shimohama S, Kihara T. Nicotinic receptor-mediated protection against beta-amyloid neurotoxicity. *Biol Psychiatry.* 2001;49:233–239.
4. Decker MW, Rueter LE, Bitner RS. Nicotinic acetylcholine receptor agonists: a potential new class of analgesics. *Curr Top Med Chem.* 2004;4:369–384.
5. Buisson B, Bertrand D. Nicotine addiction: the possible role of functional up-regulation. *Trends Pharmacol Sci.* 2002;23:130–136.
6. Pietila K, Lahde T, Attila M, Ahtee L, Nordberg A. Regulation of nicotinic receptors in the brain of mice withdrawn from chronic oral nicotine treatment. *Naunyn Schmiedebergs Arch Pharmacol.* 1998;357:176–182.
7. Rowell PP, Li M. Dose-response relationship for nicotine-induced up-regulation of rat brain nicotinic receptors. *J Neurochem.* 1997;68:1982–1989.
8. Collins AC, Romm E, Wehner JM. Dissociation of the apparent relationship between nicotine tolerance and up-regulation of nicotinic receptors. *Brain Res Bull.* 1990;25:373–379.
9. Koylu E, Demirgoren S, London ED, Pogun S. Sex difference in up-regulation of nicotinic acetylcholine receptors in rat brain. *Life Sci.* 1997;61:L185–L190.
10. Perry DC, Davila-Garcia MI, Stockmeier CA, Kellar KJ. Increased nicotinic receptors in brains from smokers: membrane binding and autoradiography studies. *J Pharmacol Exp Ther.* 1999;289:1545–1552.
11. Teaktong T, Graham AJ, Johnson M, Court JA, Perry EK. Selective changes in nicotinic acetylcholine receptor subtypes related to tobacco smoking: an immunohistochemical study. *Neuropathol Appl Neurobiol.* 2004;30:243–254.
12. Kassiou M, Eberl S, Meikle SR, et al. In vivo imaging of nicotinic receptor upregulation following chronic (-)-nicotine treatment in baboon using SPECT. *Nucl Med Biol.* 2001;28:165–175.
13. Staley JK, Krishnan-Sarin S, Cosgrove KP, et al. Human tobacco smokers in early abstinence have higher of b2* nicotinic acetylcholine receptors than non-smokers. *J Neurosci.* 2006;26:8707–8714.
14. Breese CR, Marks MJ, Logel MJ, et al. Effect of smoking history on [^{3}H]nicotine binding in human postmortem brain. *J Pharmacol Exp Ther.* 1997; 282:7–13.
15. Saji H, Ogawa M, Ueda M, et al. Evaluation of radioiodinated 5-iodo-3-(2(S)-azetidinylmethoxy)pyridine as a ligand for SPECT investigations of brain nicotinic acetylcholine receptors. *Ann Nucl Med.* 2002;16:189–200.
16. Musachio JL, Scheffel U, Finley PA, et al. 5-[I-125/123]Iodo-3(2(S)-azetidinylmethoxy)pyridine, a radioiodinated analog of A-85380 for in vivo studies of central nicotinic acetylcholine receptors. *Life Sci.* 1998;62:351–357.
17. Ueda M, Iida Y, Mukai T, et al. 5-[^{123}I]Iodo-A-85380: assessment of pharmacological safety, radiation dosimetry and SPECT imaging of brain nicotinic receptors in healthy human subjects. *Ann Nucl Med.* 2004;18: 337–344.
18. Vaupel DB, Tella SR, Huso DL, et al. Pharmacology, toxicology, and radiation dosimetry evaluation of [I-123]5-I-a-85380, a radioligand for in vivo imaging of cerebral neuronal nicotinic acetylcholine receptors in humans. *Drug Dev Res.* 2003;58:149–168.
19. Mamede M, Ishizu K, Ueda M, et al. Quantification of human nicotinic acetylcholine receptors with ^{123}I-5IA SPECT. *J Nucl Med.* 2004;45:1458–1470.
20. Marks MJ, Pauly JR, Gross SD, et al. Nicotine binding and nicotinic receptor subunit RNA after chronic nicotine treatment. *J Neurosci.* 1992;12:2765–2784.
21. Peng X, Gerzanich V, Anand R, Whiting PJ, Lindstrom J. Nicotine-induced increase in neuronal nicotinic receptors results from a decrease in the rate of receptor turnover. *Mol Pharmacol.* 1994;46:523–530.
22. Marks MJ, Burch JB, Collins AC. Genetics of nicotine response in four inbred strains of mice. *J Pharmacol Exp Ther.* 1983;226:291–302.
23. Benchcrif M, Fowler K, Lukas RJ, Lippiello PM. Mechanisms of up-regulation of neuronal nicotinic acetylcholine receptors in clonal cell lines and primary cultures of fetal rat brain. *J Pharmacol Exp Ther.* 1995;275:987–994.
24. Broussolle EP, Wong DF, Fanelli FJ, London ED. In vivo specific binding of [^{3}H]l-nicotine in the mouse brain. *Life Sci.* 1989;44:1123–1132.
25. Muzic R, Berridge M, Friedland R, Zhu N, Nelson A. PET quantification of specific binding of carbon-11-nicotine in human brain. *J Nucl Med.* 1998;39: 2048–2054.
26. Brody AL, Mandelkern MA, London ED, et al. Cigarette smoking saturates brain α4β2 nicotinic acetylcholine receptors. *Arch Gen Psychiatry.* 2006;63: 907–915.
27. Ding Y-S, Volkow ND, Logan J, et al. Occupancy of brain nicotinic acetylcholine receptors by nicotine doses equivalent to those obtained when smoking a cigarette. *Synapse.* 2000;35:234–237.
28. Collins AC, Bhat RV, Pauly JR, Marks MJ. Modulation of nicotine receptors by chronic exposure to nicotinic agonists and antagonists. *Ciba Found Symp.* 1990; 152:68–82.
29. Marks MJ, Stitzel JA, Collins AC. Time course study of the effects of chronic nicotine infusion on drug response and brain receptors. *J Pharmacol Exp Ther.* 1985;235:619–628.
30. Collins AC, Marks MJ, Pauly JR. Differential effect of chronic nicotine treatment on nicotinic receptor numbers in various brain regions of mice. *J Subst Abuse.* 1989;1:273–286.
31. Luetje CW, Patrick J. Both α and β subunits contribute to the agonist sensitivity of neuronal acetylcholine receptors. *J Neurosci.* 1991;11:837–845.
32. Fenster CP, Rains MF, Noerager B, Quick MW, Lester RAJ. Influence of subunit composition on desensitization of neuronal acetylcholine receptors at low concentrations of nicotine. *J Neurosci.* 1997;17:5747–5759.
33. Hsu Y-N, Amin J, Weiss DS, Wecker L. Sustained nicotine exposure differentially affects α3β2 and α4β2 neuronal nicotinic receptors expressed in *Xenopus* oocytes. *J Neurochem.* 1996;66:667–675.
34. Olale F, Gerznich V, Kurytov A, Wang F, Lindstrom J. Chronic nicotine exposure differentially affects the function of human α3, α4 and α7 neuronal nicotinic receptor subtypes. *J Pharmacol Exp Ther.* 1997;283:675–683.
35. Peng X, Gerzanich V, Anand R, Wang F, Lindstrom J. Chronic nicotine treatment up-regulates α3 and α7 acetylcholine receptor subtypes expressed by the human neuroblastoma cell line SH-SY5Y. *Mol Pharmacol.* 1997;51:776–784.

Eur Radiol (2007) 17: 2921–2925
DOI 10.1007/s00330-007-0688-9

NEURO

Yasutaka Fushimi
Yukio Miki
Shin-ichi Urayama
Tsutomu Okada
Nobuyuki Mori
Takashi Hanakawa
Hidenao Fukuyama
Kaori Togashi

Gray matter-white matter contrast on spin-echo T1-weighted images at 3 T and 1.5 T: a quantitative comparison study

Received: 8 August 2006
Revised: 31 January 2007
Accepted: 8 May 2007
Published online: 7 July 2007

This study was supported in part by a Health and Labour Sciences Research Grant of Japan.

Yasutaka Fushimi and Yukio Miki equally contributed to the study.

Y. Fushimi · Y. Miki (✉) · T. Okada · N. Mori · K. Togashi
Department of Diagnostic Imaging and Nuclear Medicine, Kyoto University Graduate School of Medicine,
54 Shogoin-Kawaharacho, Sakyo-ku, Kyoto, 606-8507, Japan
e-mail: mikiy@kuhp.kyoto-u.ac.jp
Tel.: +81-75-7513710
Fax: +81-75-7719709

S.-i. Urayama · T. Hanakawa · H. Fukuyama
Human Brain Research Center, Kyoto University Graduate School of Medicine,
Kyoto, Japan

T. Hanakawa
Department of Cortical Function Disorders, National Institute of Neuroscience, National Center of Neurology and Psychiatry,
Kyoto, Japan

Abstract Discrepancies exist in the literature regarding contrast between gray and white matter on spin-echo (SE) T1-weighted MR imaging at 3 T. The present study quantitatively assessed differences in gray matter-white matter contrast on both single- and multi-slice SE T1-weighted imaging between 3 and 1.5 T. SE T1-weighted sequences with the same parameters at both 3 and 1.5 T were used. Contrast-to-noise ratio (CNR) between gray and white matter ($CNR_{GM\text{-}WM}$) was evaluated for both frontal lobes. To assess the effects of interslice gap, multi-slice images were obtained with both 0 and 25% interslice gap. Single-slice $CNR_{GM\text{-}WM}$ was higher at 3 T (17.66±2.68) than at 1.5 T (13.09±2.35; $P<0.001$). No significant difference in $CNR_{GM\text{-}WM}$ of multi-slice images with 0% gap was noted between 3 and 1.5 T (3T, 8.61±2.55; 1.5T, 7.43±1.20; $P>0.05$). Multi-slice $CNR_{GM\text{-}WM}$ with 25% gap was higher at 3T (12.47±3.31) than at 1.5 T (9.73±1.37; $P<0.001$). $CNR_{GM\text{-}WM}$ reduction rate of multi-slice images with 0% gap compared with single-slice images was higher at 3T (0.47±0.13) than at 1.5 T (0.38±0.09; $P=0.02$). $CNR_{GM\text{-}WM}$ on single-slice SE T1-weighted imaging and $CNR_{GM\text{-}WM}$ on multi-slice images with 25% interslice gap were better at 3 T than at 1.5 T. The influence of multi-slice imaging on $CNR_{GM\text{-}WM}$ was significantly larger at 3T than at 1.5 T.

Keywords High-field MR · Brain · Magnetic resonance imaging · T1-weighted image

Introduction

Magnetic resonance (MR) imaging at 3 T has gradually been introduced to clinical practice in addition to research fields. Signal-to-noise ratio (SNR) is better at 3 T MR imaging than at 1.5 T MR imaging [1–4]. This improved SNR at 3 T MR imaging provides advantages in various applications [5–7]. Increased T1 relaxation time and improved SNR at 3 T provide better visualization on MR angiography [8, 9].

Discrepancies exist in the literature regarding contrast between gray matter (GM) and white matter (WM) on spin-echo (SE) T1-weighted MR imaging at 3 T. Nobauer-Huhmann et al. [10] reported that visual assessment of

differentiation between GM and WM on SE T1-weighted sequences was significantly lower at 3 T than at 1.5 T. They noted that the repetition time (TR) optimized for 1.5 T was too long to obtain sufficient contrast between GM and WM at 3 T. A review by Scarabino et al. [11] stated that SE T1-weighted images show low contrast-to-noise ratio (CNR) between GM and WM (CNR_{GM-WM}), probably due to longer T1 relaxation time at 3T. Sasaki et al. [12] commented that delayed magnetization recovery due to longer T1 relaxation time reduces contrast between GM and WM on SE T1-weighted imaging at 3 T. Ross [13] indicated in an editorial that quality of SE T1-weighted imaging is degraded by longer T1 relaxation time and chemical shift. Conversely, Lu et al. [14] recently published data showing CNR_{GM-WM} increased by 20.7% on SE T1-weighted imaging at 3T compared with CNR_{GM-WM} at 1.5 T by optimizing imaging parameters for each magnet. In addition, Schmitz et al. [15] demonstrated that SE T1-weighted imaging could display better CNR at 3 T by adjusting flip angles.

To the best of our knowledge, no comparison studies featuring CNR_{GM-WM} of SE T1-weighted sequences with the same imaging parameters at 3 and 1.5 T have been reported. Differences in CNR_{GM-WM} between single- and multi-slice SE T1-weighted sequences have also not been well studied for 3 and 1.5 T.

The present study quantitatively examined differences in CNR_{GM-WM} for both single- and multi-slice SE T1-weighted images using the same imaging parameters between 3 and 1.5 T.

Materials and methods

Subjects

Subjects comprised 10 healthy volunteers (7 males, 3 females, range 25–36 years, average 29 years). All subjects were neurologically examined by a neurologist (T.H.) and were considered neurologically healthy. The local ethical committee approved the study protocols, and all subjects provided written informed consent before entering the study.

Imaging protocols

All subjects underwent both 3 and 1.5 T imaging on the same day in random order, using a 3 T MR scanner (Magnetom Trio, Siemens, Erlangen, Germany) and a 1.5 T MR scanner (Magnetom Symphony, Siemens, Erlangen, Germany). The interval between imagings was <30 min. The body coil was not standard equipment at 3 T; therefore, the head coil was used as a transmission coil. The standard setup of body coil transmission was used at 1.5 T. The image center was shared between both MR units by posting markers on the face of each subject. A circular polarized head coil was used, and the head was firmly fixed using foam pads. Subjects were instructed not to move during MR imaging. Imaging slices were positioned parallel to the anterior commissure-posterior commissure line at the level of the basal ganglia.

Imaging parameters

SE T1-weighted sequence that was routinely used at 1.5 T was applied for both 3 and 1.5 T imaging: TR 600 ms; echo time (TE) 20 ms; slice thickness 5 mm; number of averages 1; matrix 256×256; flip angle 90°; bandwidth 90 Hz; scan time 2 min 38 s. Within each subject, this sequence was repeated with the image center fixed for the single slice, multi-slice with 0% gap (gapless), and multi-slice with 25% interslice gap (1.25-mm interslice gap) (Fig. 1). The number of multi-slice images was set as seven due to high systemic absorption rate (SAR) at 3 T.

Analysis of regions of interest

GM and WM of frontal lobes and background were selected as regions of interest (ROI) on the center slice of each SE T1-weighted image (Fig. 2). In each subject, the same ROIs were applied for all images. CNR_{GM-WM} was defined as the difference between intensities of GM and WM divided by the standard deviation of the background [16]. ROIs were drawn using ImageJ software (National Institutes of Health, Bethesda, MD, USA).

Statistical analysis

Two-sided paired *t*-test was applied using JMP 5.1 (SAS Institute, Cary, NC, USA). Values of $P<0.05$ were considered statistically different.

Results

Single-slice CNR_{GM-WM} was significantly higher at 3 T (17.66±2.68) than at 1.5 T (13.09±2.35) ($P<0.001$) (Fig. 3). A 1.37±0.23-fold gain in CNR_{GM-WM} was seen for single slice at 3 T compared with 1.5 T.

No significant difference in multi-slice CNR_{GM-WM} was noted with 0% gap (3 T: 8.61±2.55; 1.5T: 7.43±1.20; $P>0.05$) between 3 and 1.5 T. Multi-slice CNR_{GM-WM} with 25% gap was higher at 3 T (12.47±3.31) than at 1.5 T (9.73±1.37; $P<0.001$) (Fig. 3).

CNR_{GM-WM} reduction rate for multi-slice with 0% gap from single-slice was higher at 3 T (0.47±0.13) than at

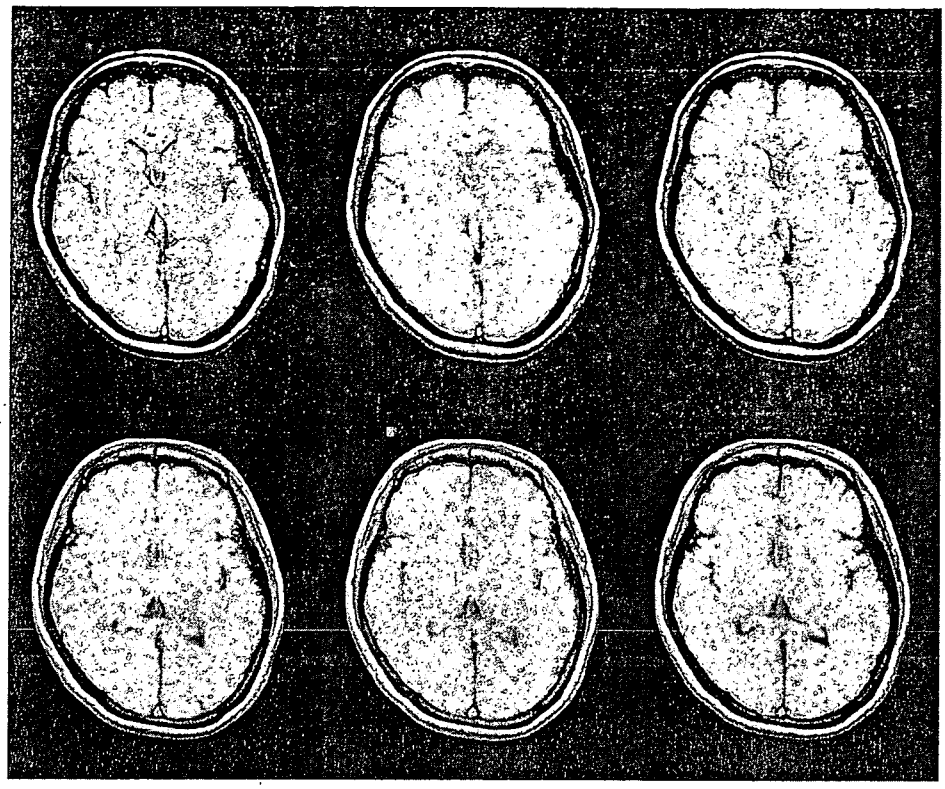

Fig. 1 SE T1-weighted imaging at 3 T (*upper row*) and 1.5 T (*lower row*). From *left* to *right*, total imaging slices are 1 (single slice), multi-slices with 0% interslice gap, and multi-slices with 25% interslice gap. Contrast between GM and WM at 3 and 1.5 T is more conspicuous in a single slice than in multi-slices. Contrast between GM and WM of a single slice is obviously better at 3 T than at 1.5 T. Contrast between GM and WM for multi-slices with 25% interslice gap is better at 3 T than at 1.5 T

1.5 T (0.38±0.09; P=0.02) (Fig. 4). No significant difference in $CNR_{GM\text{-}WM}$ reduction rate was seen for multi-slice with 25% gap from single slice (3 T: 0.29±0.16; 1.5 T: 0.28±0.10; P>0.05) between 3 and 1.5 T (Fig. 4).

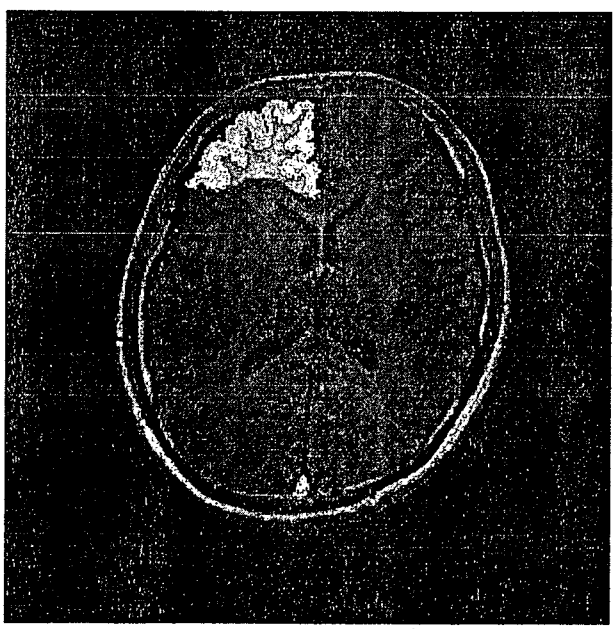

Fig. 2 A representative image of ROI on SE T1-weighted image. GM and WM of frontal lobes were selected as ROI

Discussion

Single-slice SE T1-weighted imaging produced better $CNR_{GM\text{-}WM}$ at 3 T than at 1.5 T in this study. Under the same imaging parameters for both magnetic fields, $CNR_{GM\text{-}WM}$ increased 1.37±0.23-fold at 3 T compared to 1.5 T. Lu et al. [14] reported a 20.7% increase in $CNR_{GM\text{-}WM}$ on SE T1-weighted imaging at 3 T compared with 1.5 T in five volunteers; however, imaging parameters for SE T1-weighted imaging were optimized for each magnet in their study. In this study, the same imaging parameters were applied for SE T1-weighted imaging at both 3 and 1.5 T, and better $CNR_{GM\text{-}WM}$ was seen at 3 T compared with 1.5 T. To the best of our knowledge, this is the first comparison study featuring differences in $CNR_{GM\text{-}WM}$ on SE T1-weighted imaging using the same imaging parameters at 3 and 1.5 T.

$CNR_{GM\text{-}WM}$ was decreased in multi-slice imaging with 0% gap for both magnetic fields when compared to single-slice imaging, and a larger $CNR_{GM\text{-}WM}$ reduction rate for multi-slices with 0% gap from single slice was observed at 3 T than at 1.5 T. This might be due to cross-talk effect and/or magnetization transfer (MT) effect, both of which may reduce CNR with multi-slice imaging [17]. MT effect is reportedly higher at 3 T than at 1.5 T [18, 19], partially supporting our results.

In this study, both multi-slice and gapless imaging exacerbated $CNR_{GM\text{-}WM}$ on SE T1-weighted sequences, and the degree of $CNR_{GM\text{-}WM}$ reduction was larger at 3T

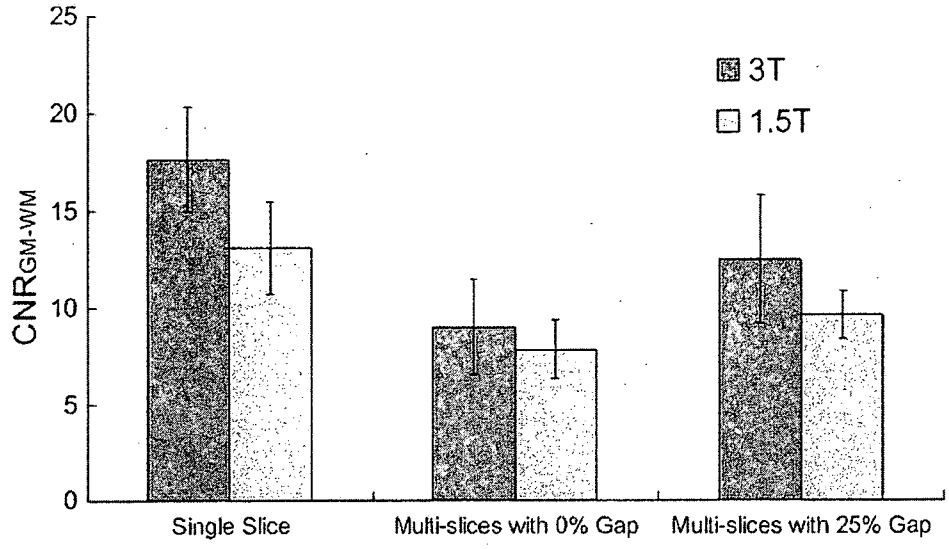

Fig. 3 $CNR_{GM\text{-}WM}$ for single slice, multi-slice with 0% gap, and multi-slice with 25% gap at 3 T (*dark gray bar*) and 1.5 T (*light gray bar*). *Error bars* represent standard deviation. Single-slice $CNR_{GM\text{-}WM}$ was higher at 3 T (17.66±2.68) than at 1.5 T (13.09±2.35; $P<0.001$). Multi-slice $CNR_{GM\text{-}WM}$ with 25% gap was higher at 3T (12.47±3.31) than at 1.5 T (9.73±1.37; $P<0.001$). No significant difference in multi-slice $CNR_{GM\text{-}WM}$ with 0% gap was noted between 3 T and 1.5 T (3T: 8.61±2.55; 1.5 T: 7.43±1.20; $P>0.05$)

than at 1.5 T. Attention must therefore be paid to the interslice gap in applying SE T1-weighted sequences at 3 T. The best $CNR_{GM\text{-}WM}$ at 3 T was obtained using single-slice imaging in this study, which of course will not likely be applicable in routine practice. However, radiologists need to know that $CNR_{GM\text{-}WM}$ on SE T1-weighted sequences is better at 3 T than at 1.5 T without the influences of multi-slice imaging. 3D gradient sequences such as magnetization prepared rapid acquisition with gradient echo (MPRAGE) or fast spoiled gradient echo (FSPGR) sequences are often used as substitutes for SE T1-weighted sequences at 3 T [10, 12], but SE T1-weighted imaging may be applicable at 3 T if sufficient interslice gap is applied and if the SAR issue is addressed.

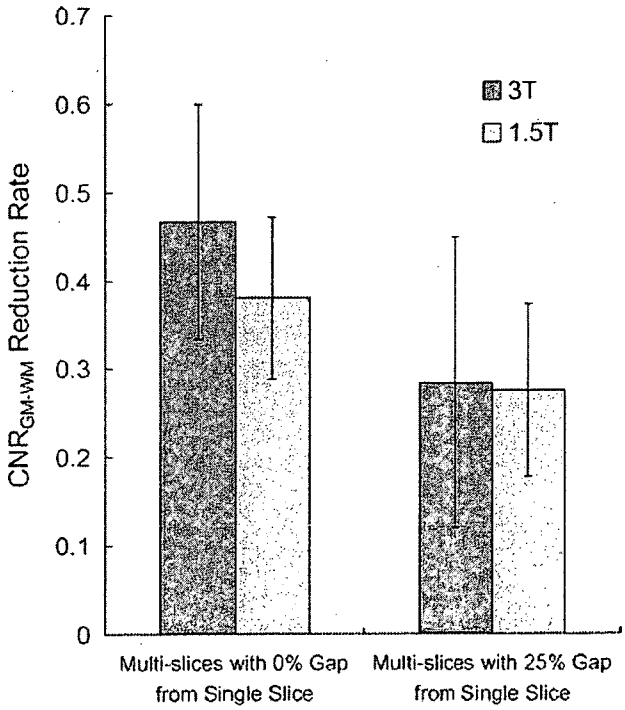

Fig. 4 $CNR_{GM\text{-}WM}$ reduction rate for multi-slice imaging with 0% gap from single-slice imaging at 3 T (*dark gray bar*) and 1.5 T (*light gray bar*). *Error bars* represent standard deviation. $CNR_{GM\text{-}WM}$ reduction rate is significantly larger at 3 T (0.47±0.13) than at 1.5 T (0.38±0.09; $P=0.02$). $CNR_{GM\text{-}WM}$ reduction rates for multi-slices with 25% gap from single-slice imaging at 3 T (*dark gray bar*) and 1.5 T (*light gray bar*) are shown. No significant difference in $CNR_{GM\text{-}WM}$ reduction rate is noted (3 T: 0.29±0.16; 1.5 T: 0.28±0.10; $P>0.05$

Relatively lower contrast between GM and WM at 3 T has been reported by various authors [10–13], but these reports have mainly been based on visual assessment. In the present study, differences in $CNR_{GM\text{-}WM}$ on SE T1-weighted imaging between 1.5 and 3 T were quantitatively evaluated for the first time. Since the intensity of the center part of images on SE T1-weighted sequences at 3 T is higher than the peripheral parts, probably due to B1 homogeniety [20, 21], display window-width could be set wider so that the center of images will not be whited-out, an effect which might prevent radiologists from noticing the true contrast between GM and WM at 3 T. Schmitz et al. [15] revealed that SE T1-weighted imaging with lower flip angles contributes to better CNR at 3 T probably because of more uniform signal intensity distribution. They achieved SE T1-weighted imaging with lower SAR at 3 T by decreasing flip angles. They also commented that there might be other factors that decrease CNR, such as magnetization transfer or shielding effects [15]. Lu et al. [14] reported that TR had more influence on $CNR_{GM\text{-}WM}$ of SE T1-weighted images at 3 T than TE. They optimized SE T1-weighted images at 3 T by plotting CNR of T1-weighted images with various TR and TE, which showed better $CNR_{GM\text{-}WM}$ than that at 1.5 T [14].

The present study displays some limitations. Identical imaging parameters were applied for 3 T SE T1-weighted sequence as for 1.5 T, which is routinely used in clinical

practice, a whole brain was not covered, and total imaging slices were limited to conform to SAR limitations at 3 T. Future studies need to optimize SE T1-weighted sequences at 3 T to obtain more imaging slices with suitable CNR_{GM-WM}, so that SE T1-weighted sequences can be routinely used at 3 T. According to the results of the present study, a two package of interleaved SE T1-weighted imaging with 100% interslice gap that will cover the whole brain might show better CNR_{GM-WM} at 3 T. In clinical practices, SE T1-weighted imaging with reduced interslice gaps or with lower flip angles might show better CNR_{GM-WM} at 3 T, however, further investigation should be done in future studies.

One possible reason for the differences in CNR_{GM-WM} on SE T1-weighted imaging between 1.5 and 3 T is that a body coil was used for transmitting at 1.5 T, whereas at 3 T a head coil was used, which is known to have poorer transmission efficiency and B1 homogeneity than a body coil.

In conclusion, CNR_{GM-WM} on single-slice SE T1-weighted imaging and CNR_{GM-WM} on multi-slice imaging with 25% interslice gap are better at 3 T than at 1.5 T. The influence of multi-slice imaging on CNR_{GM-WM} is significantly larger at 3 T than at 1.5 T.

References

1. Hoenig K, Kuhl CK, Scheef L (2005) Functional 3.0-T MR assessment of higher cognitive function: are there advantages over 1.5-T imaging? Radiology 234:860–868
2. Manka C, Traber F, Gieseke J, Schild HH, Kuhl CK (2005) Three-dimensional dynamic susceptibility-weighted perfusion MR imaging at 3.0 T: feasibility and contrast agent dose. Radiology 234:869–877
3. Frayne R, Goodyear BG, Dickhoff P, Lauzon ML, Sevick RJ (2003) Magnetic resonance imaging at 3.0 Tesla: challenges and advantages in clinical neurological imaging. Invest Radiol 38:385–402
4. Schick F (2005) Whole-body MRI at high field: technical limits and clinical potential. Eur Radiol 15:946–959
5. Moser E, Trattnig S (2003) 3.0 Tesla MR systems. Invest Radiol 38:375–376
6. Kuhl CK, Textor J, Gieseke J, von Falkenhausen M, Gernert S, Urbach H, Schild HH (2005) Acute and subacute ischemic stroke at high-field-strength (3.0-T) diffusion-weighted MR imaging: intraindividual comparative study. Radiology 234:509–516
7. Okada T, Miki Y, Fushimi Y, Hanakawa T, Kanagaki M, Yamamoto A, Urayama S, Fukuyama H, Hiraoka M, Togashi K (2006) Diffusion-tensor fiber tractography: intraindividual comparison of 3.0-T and 1.5-T MR imaging. Radiology 238:668–678
8. Bernstein MA, Huston J 3rd, Lin C, Gibbs GF, Felmlee JP (2001) High-resolution intracranial and cervical MRA at 3.0T: technical considerations and initial experience. Magn Reson Med 46:955–962
9. Fushimi Y, Miki Y, Kikuta K, Okada T, Kanagaki M, Yamamoto A, Nozaki K, Hashimoto N, Hanakawa T, Fukuyama H, Togashi K (2006) Comparison of 3.0- and 1.5-T three-dimensional time-of-flight MR angiography in Moyamoya disease: preliminary experience. Radiology 239:232–237
10. Nobauer-Huhmann IM, Ba-Ssalamah A, Mlynarik V, Barth M, Schoggl A, Heimberger K, Matula C, Fog A, Kaider A, Trattnig S (2002) Magnetic resonance imaging contrast enhancement of brain tumors at 3 tesla versus 1.5 tesla. Invest Radiol 37:114–119
11. Scarabino T, Nemore F, Giannatempo GM, Bertolino A, Di Salle F, Salvolini U (2003) 3.0 T magnetic resonance in neuroradiology. Eur J Radiol 48:154–164
12. Sasaki M, Inoue T, Tohyama K, Oikawa H, Ehara S, Ogawa A (2003) High-field MRI of the central nervous system: current approaches to clinical and microscopic imaging. Magn Reson Med Sci 2:133–139
13. Ross JS (2004) The high-field-strength curmudgeon. AJNR Am J Neuroradiol 25:168–169
14. Lu H, Nagae-Poetscher LM, Golay X, Lin D, Pomper M, van Zijl PC (2005) Routine clinical brain MRI sequences for use at 3.0 Tesla. J Magn Reson Imaging 22:13–22
15. Schmitz BL, Gron G, Brausewetter F, Hoffmann MH, Aschoff AJ (2005) Enhancing gray-to-white matter contrast in 3 T T1 spin-echo brain scans by optimizing flip angle. AJNR Am J Neuroradiol 26:2000–2004
16. Constable RT, Henkelman RM (1991) Contrast, resolution, and detectability in MR imaging. J Comput Assist Tomogr 15:297–303
17. Majumdar S, Sostman HD, MacFall JR (1989) Contrast and accuracy of relaxation time measurements in acquired and synthesized multislice magnetic resonance images. Invest Radiol 24:119–127
18. Schmitz BL, Aschoff AJ, Hoffmann MH, Gron G (2005) Advantages and pitfalls in 3T MR brain imaging: a pictorial review. AJNR Am J Neuroradiol 26:2229–2237
19. Stanisz GJ, Odrobina EE, Pun J, Escaravage M, Graham SJ, Bronskill MJ, Henkelman RM (2005) T1, T2 relaxation and magnetization transfer in tissue at 3T. Magn Reson Med 54:507–512
20. Vaughan JT, Garwood M, Collins CM, Liu W, DelaBarre L, Adriany G, Andersen P, Merkle H, Goebel R, Smith MB, Ugurbil K (2001) 7 T vs. 4 T: RF power, homogeneity, and signal-to-noise comparison in head images. Magn Reson Med 46:24–30
21. Collins CM, Liu W, Schreiber W, Yang QX, Smith MB (2005) Central brightening due to constructive interference with, without, and despite dielectric resonance. J Magn Reson Imaging 21:192–196

Heterospecific and conspecific social cognition in the anterior cingulate cortex

Jun Shinozaki[a], Takashi Hanakawa[a,b] and Hidenao Fukuyama[a]

[a]Human Brain Research Center, Kyoto University Graduate School of Medicine, Kyoto and [b]Department of Cortical Function Disorders, National Center of Neurology and Psychiatry, Kodaira, Tokyo, Japan

Correspondence to Dr Takashi Hanakawa, MD, PhD, Section Chief, Department of Cortical Function Disorders, National Institute of Neuroscience, National Center of Neurology and Psychiatry, 4-1-1 Ogawahigashi, Kodaira, Tokyo 187-8502, Japan
Tel: +81 42 341 2711 (ext) 5173; fax: +81 42 346 1748; e-mail: hanakawa@ncnp.go.jp

Received 3 March 2007; accepted 21 March 2007

The development of human social cognition has allowed interactions with other species and the formation of a cooperative multispecies society. This feature posited keen attention on the following question: is heterospecific social cognition represented in the same brain areas as conspecific social cognition? Here we investigated brain activity accompanying the facial recognition of familiar humans and of companion dogs, both of whom had real social interactions with participants. The rostroventral anterior cingulate cortex responded to both species whereas the caudal anterior cingulate cortex was sensitive only to familiar humans. Social cognition processes may be dual-layered: the rostroventral anterior cingulate cortex is associated with fundamental and intuitive aspects, whereas the caudal anterior cingulate cortex is concerned with the analysis of complex social interactions. *NeuroReport* 18:993–997 © 2007 Lippincott Williams & Wilkins.

Keywords: anterior cingulate cortex, conspecific, facial recognition, functional MRI, heterospecific, social cognition

Introduction

Animals that form societies, particularly humans, have developed the ability to deal with complex interindividual relationships through social cognition [1]. Although these interactions typically occur between conspecifics, they can also extend to heterospecifics [2]. One example is the social interaction that occurs between humans and companion animals, which are often treated like family members. Many humans receive emotional support from companion species [3] and have sincere concern for their welfare [4]. Interactions with animals might also help children to develop empathetic ability [5]. Thus, it seems to be important to know the neural mechanisms underlying heterospecific social interactions or the roles of cognition and emotion in this process.

Recent imaging studies have begun to explore the neural underpinnings of conspecific social cognition using various tasks, including face recognition [6]. Faces convey critical information for social cognition, as the recognition of individuals and their emotional states constitute the fundamentals of interpersonal relationships [1]. In particular, recognizing familiar faces, such as those of family members, activates the amygdala [7] and the medial prefrontal areas, including the anterior cingulate cortex [8]. Parts of the anterior cingulate cortex are rich in spindle-shaped output neurons that are present in great apes [9]. In addition, abundant connections with the limbic and prefrontal areas render the anterior cingulate cortex adequate for representing society [10], including the family, which is one of its most critical constituents. The anterior cingulate cortex can be divided into the affective rostroventral anterior cingulate cortex and the cognitive caudal anterior cingulate cortex [11]. Several types of activity were expected to occur in the anterior cingulate cortex during the recognition of heterospecific and conspecific family members. We hypothesized that faces of human and canine 'family' members would evoke similar responses in the rostroventral anterior cingulate cortex, which might support the processing of social information closely related to emotion. In addition, we predicted that the recognition of familiar human faces would evoke complex cognitive reflection, which might involve the analytical caudal anterior cingulate cortex regions [11–14].

Materials and methods

Participants

Seventeen healthy volunteers (11 men and six women) participated in this study. All participants had one or two companion dogs and none reported critical family problems. Four additional volunteers (one woman) participated in a control experiment for recognition of familiar objects. All individuals gave written informed consent to participate in the study and the protocol was approved by the local ethics committee.

Stimuli

The stimuli comprised grayscale digital photographs of faces and mosaic patterns. Luminance and contrast were roughly adjusted across the stimuli. In total, six types of face stimulus were prepared specifically for each participant: family, newly learned and unfamiliar human faces (FH, NH

and UH, respectively), and family, newly learned and unfamiliar dog faces (FD, ND and UD, respectively). The human facial expressions ranged from neutral to a faint smile. Two types of mosaic pattern were created: newly learned mosaics (NM) and unfamiliar mosaics (UM). The numbers of face and mosaic images in each category varied from 14 to 20, according to availability. Each stimulus subtended visual angles of ~10° vertically and horizontally. All facial stimuli were superimposed onto a white background of 640 × 480 pixel size, after removing the original backgrounds of the photographs. Similarly, pictures of personally familiar and newly learned objects were prepared for the object-recognition experiment. The objects were personal belongings such as cell phones. The stimuli were presented for 300 ms in a semirandom order and the interstimulus intervals were varied between 5 and 10 s.

Experimental procedures

Participants were asked to memorize a predetermined set of stimuli, consisting of NH, ND and NM. To assess the complete memorization of NH, ND and NM, participants saw pictures of FH, FD, NH, ND, NM and UM (18 pictures in total) and judged whether they knew them or not before the imaging experiment. During scanning, the stimulus presentation was controlled by a personal computer synchronized with the MRI scanner. The onset of the stimulus presentation was semirandomly staggered with the acquisition onset of each functional image. In the MRI scanner, the participants judged whether they had previously seen the presented images and reported their answer by pressing one of the two buttons. The accuracy and response times were recorded. The participants maintained visual fixation on a crosshair at baseline. In total, 439 volumes were acquired in each imaging run (18 min 17.5 s). Two imaging runs were administered for each participant. The same stimulus was not presented twice within a single run and stimuli from unfamiliar categories were not repeated in the second run.

After the functional MRI (fMRI), the participants reported on how much support they received everyday from their human family members and companion dogs, using the Scale of Expectancy for Social Support (SESS) [15] and the Animal Companionship and Support Scale (ACSS) [16], respectively. Nine participants also rated subjective valence and arousal to each facial stimulus, using scales ranging from 1 (most negative or least arousal) to 9 (most positive or most arousal).

Image acquisition

FMRI experiments were conducted on a 3-T scanner equipped with a volume headcoil (Siemens Trio, Erlangen, Germany). Functional images were obtained in a T2*-weighted gradient-echo echo-planar imaging sequence with prospective motion correction. The image-acquisition parameters were as follows: repetition time (TR) = 2.5 s; echo time (TE) = 30 ms; flip angle (FA) = 90°; field of view (FOV) = 192 mm; matrix = 64 × 64; 40 interleaved axial slices with 3-mm thickness without gaps (3-mm cubic voxels). The first two volumes were not saved to allow for signal stabilization.

For anatomic images, T1-weighted three-dimensional structural images were also obtained using a magnetization-prepared rapid-gradient echo sequence. Each participant lay supine on a scanner bed, with a button-response device held in the right hand. The participants viewed visual stimuli that were back-projected onto a screen through a built-in mirror. Foam pads were used to minimize head motion.

Image analysis

The fMRI data were analyzed with SPM2 (Wellcome Department of Imaging Neuroscience, University College London, London, UK) implemented on MATLAB 6.5 (MathWorks, Natick, Massachusetts, USA), using the principles of the general linear model [17]. The functional images were corrected for differences in slice-acquisition timing and were then spatially realigned to the first image of the initial run to adjust for residual head movements after prospective motion correction. The realigned images were spatially normalized to fit to a Montreal Neurological Institute template [18] based on the standard stereotaxic coordinate system [19]. Subsequently, all images were smoothed with an isotropic Gaussian kernel of 12-mm full-width at half-maximum. Each of the eight stimulus conditions was separately modeled as a regressor for the first-level multiregression analysis. This analysis was performed for each participant, to test the correlation between the MRI signals and a train of delta functions (representing event onsets) convolved with the canonical hemodynamic response function and its temporal derivative. Global signal normalization was performed only between runs. Low-frequency noise was removed using a high-pass filter with a cutoff of 128 s and serial correlation was adjusted using an AR(1) model. By applying the appropriate linear contrast to the parameter estimates, mean-effect images reflecting the magnitude of correlation between the signals and the model of interest were computed. These were used for the subsequent second-level random-effect model analysis. Group-level statistical parametric maps were produced using the one-sample *t*-test.

For the correlation analysis, the raw SESS and ACSS scores were used as regressors at the second level. The statistical parametric map (SPM){*t*} was first thresholded at $P < 0.001$ and the significance of the activity was defined by the cluster-level P value corrected for multiple comparisons for the entire brain ($P < 0.05$). For the caudal anterior cingulate cortex, a small volume correction analysis was applied (false discovery rate corrected, $P < 0.05$) for both the interaction and correlation analyses. The center coordinates ($x = -9$, $y = 6$, $z = 42$) of a spherical region-of-interest with a 7.5 mm radius was determined on the basis of a previous report [13] showing the relationship of the caudal anterior cingulate cortex with higher-order interindividual interactions. The resulting activation maps were displayed on the anatomically normalized mean T1 image derived from all participants, to identify the anatomical correlates of the activity. The results are reported on the basis of the coordinates of the Montreal Neurological Institute template.

Results

Behavioral results

The accuracy was on average over 90% for all stimuli. A Wilcoxon signed-rank test was used to analyze the hit rates. No significant differences were found in the hit rates during fMRI between FH and NH ($P = 0.480$), or between FD and ND ($P = 0.686$). The hit rates demonstrated similar levels of robustness in the familiarity of recognizable faces between the human and dog conditions. The averaged response

times were 762, 799, 774 and 871 ms for FH, NH, FD and ND, respectively. The response times were analyzed with two-way repeated-measure analysis of variance (ANOVA) followed by Bonferroni's posthoc two-tailed *t*-test. Significant effects of both familiarity and species were noted on response times ($P<0.001$ and $=0.003$, respectively). Specifically, the response to FH and FD tasks was significantly faster than that to NH and ND tasks ($P=0.034$ and 0.001, respectively).

Species-invariant and human-selective activities

To explore specific family-related activity, the familial and newly learned faces were contrasted separately for the conspecific (FH minus NH) and heterospecific (FD minus ND) conditions. Conjunction analyses revealed species-invariant activation during familial face recognition only in the rostroventral anterior cingulate cortex (coordinates: $x=-12$, $y=32$, $z=-12$; Z-value = 4.34) at the whole-brain corrected threshold ($P<0.05$; Fig. 1a). Interaction analyses were then conducted to identify familial human-selective activity (conspecific minus heterospecific) or dog-selective activity (heterospecific minus conspecific). The former was identified in the caudal anterior cingulate cortex (coordinates: $x=-8$, $y=12$, $z=44$; Z-value = 3.13) (Fig. 1b) after a small volume correction ($P<0.05$), whereas the latter did not reach statistical significance.

Psychological scales and anterior cingulate cortex activities

The imaging data (e.g. FH relative to baseline) were reanalyzed to identify any brain activity that covaried with these scores. Participants with higher perceived ACSS scores showed increased activity in the rostroventral anterior cingulate cortex, right anterior insula and pulvinar during FD recognition (Fig. 2b). The ACSS-correlated rostroventral anterior cingulate cortex region overlapped with that showing species-invariant rostroventral anterior cingulate cortex activity during familial face recognition. The SESS scores were positively correlated with caudal anterior cingulate cortex activity during FH recognition (Fig. 2c). This relationship was statistically significant after a small volume correction ($P<0.05$). This further supported the role of the caudal anterior cingulate cortex in processing only human interpersonal relationships. A confirmation analysis upheld the specificity of these correlations; there was no correlation between the caudal anterior cingulate cortex activity during family dog recognition and the ACSS score ($r=0.387$, $P=0.124$), or between the rostroventral anterior cingulate cortex activity during family human recognition and the SESS score ($r=0.143$, $P=0.583$).

The observed medial frontal activities could not be attributed to task difficulty, as the FH and FD tasks were relatively easier than the NH and ND tasks according to the response-time analysis. To determine whether valence or arousal differences could account for our findings, nine participants rated these parameters for each stimulus after the fMRI. The results showed that familiarity and species had no significant effects on the arousal rating ($P=0.095$ and 0.088, respectively). Significant effects on the valence rating were, however, observed for familiarity ($P=0.004$) and species ($P=0.039$). Valence was rated more positively for the family face condition than the other conditions ($P=0.014$ versus newly learned, $P=0.008$ versus unfamiliar). Notably, the overall effect of species was primarily due to the significantly higher valence ratings for UD than for UH ($P=0.005$). Brain activity was thus compared between UD and UH in the rostroventral and caudal anterior cingulate areas to examine the general effects of valence. Despite the significant valence disparity, the brain activity in the UD and UH conditions did not differ in the rostroventral anterior cingulate cortex ($P=0.351$) or the caudal anterior cingulate cortex ($P=0.130$). Thus, the arousal or simple valence component alone appeared unable to explain the observed rostroventral and caudal anterior cingulate cortex activities.

Finally, to ensure that the anterior cingulate activities did not merely reflect different degrees of familiarity, brain activity was compared between the newly learned and unknown faces. Simple familiarity-related activation was not detected in the medial frontal area according to this

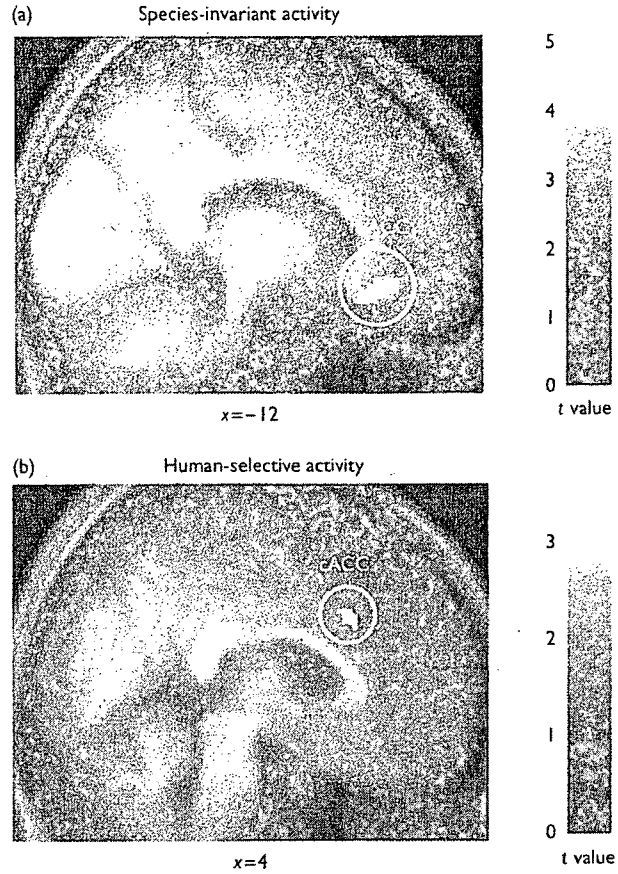

Fig. 1 Species-invariant and human-selective activities in the anterior cingulate cortex. (a) Species-invariant activity coequally associated with the recognition of familial human and canine faces was detected in the rostroventral anterior cingulate cortex (rvACC; coordinates, $x=-12$, $y=32$, $z=-12$; Z-value = 4.34) at a cluster-level corrected threshold of $P<0.05$. (b) Human-selective activity during the recognition of familial faces was found in the caudal anterior cingulate cortex (cACC; coordinates, $x=-8$, $y=12$, $z=44$; Z-value = 3.13) at a false discovery rate corrected threshold of $P<0.05$ after a small volume correction. When a uniform threshold of uncorrected $P<0.001$ was applied, the numbers of activated voxels were 244 and 51 in the rostroventral anterior cingulate cortex and the caudal anterior cingulate cortex, respectively. Activity is shown at a height threshold of $P<0.001$ (uncorrected) with an extent threshold of 50 voxels.

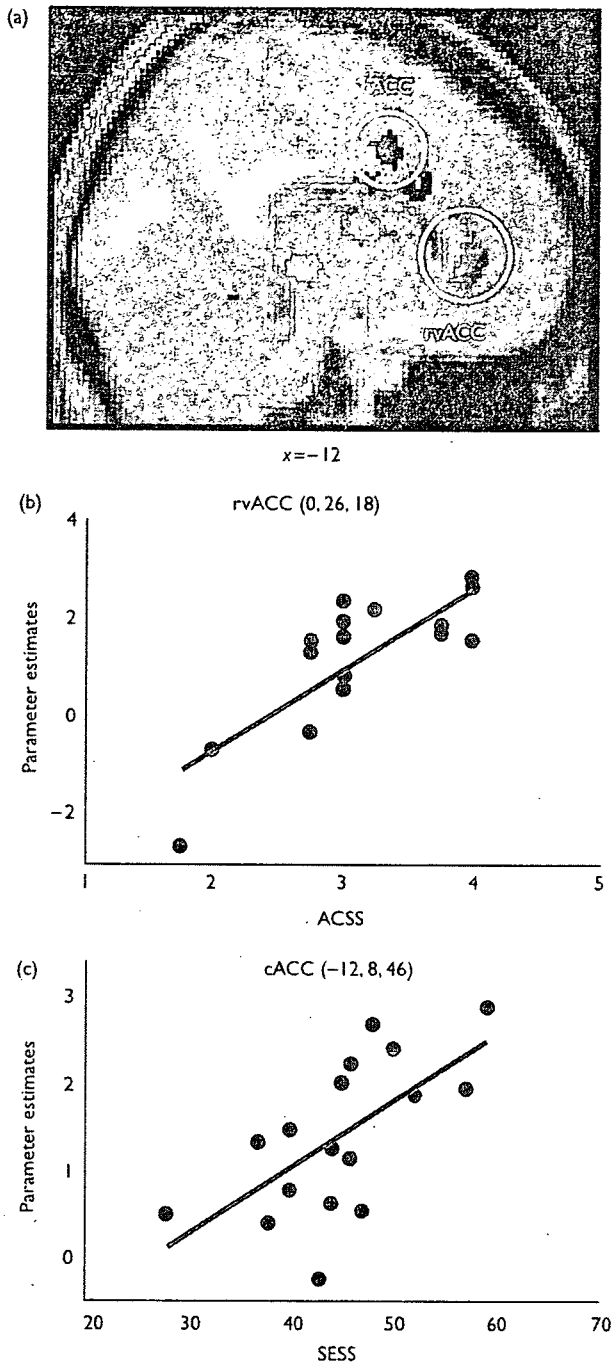

Fig. 2 Correlation between anterior cingulate cortex activities and support from family members or companion dogs. (a) Brain activity correlated with the Scale of Expectancy for Social Support (SESS) scores for human family members is shown in green. This activity was significant during human familial face recognition in the caudal anterior cingulate cortex (cACC) after a small volume correction ($P < 0.05$). Brain activity correlated with the Animal Companionship and Support Scale (ACSS) scores is shown in red. This activity was significant in the rostroventral anterior cingulate cortex (rvACC) at a cluster-level corrected threshold for the whole brain ($P < 0.05$). The SESS-correlated activity was thresholded at uncorrected $P < 0.025$, and the ACSS-correlated activity was thresholded at uncorrected $P < 0.005$ for display purposes. (b) The rostroventral anterior cingulate cortex activity during family dog recognition was significantly correlated with the ACSS score ($r = 0.805$, $P < 0.001$). (c) The caudal anterior cingulate cortex activity during familial human recognition was positively correlated with the SESS score ($r = 0.639$, $P = 0.006$).

confirmatory analysis ($P < 0.01$, uncorrected). To assess the possible effects of nonsocial, long-term familiarity, brain activity was compared between personally familiar and newly learned objects in four participants. Long-term familiarity to nonliving objects did not significantly activate the medial frontal area in a fixed-effect model group analysis ($P < 0.01$, uncorrected). These additional data further supported the hypothesis that the rostroventral and caudal anterior cingulate activities more likely reflected long-term social familiarity than different degrees of familiarity or long-term nonsocial familiarity.

Discussion

At least two distinct activities were identified in the anterior cingulate cortex during the recognition of human and canine faces associated with long-term social familiarity: species-invariant activity corresponding to the affective rostroventral anterior cingulate cortex and species-selective activity corresponding to the cognitive caudal anterior cingulate cortex. Recently, the medial prefrontal cortex was shown to be active during the analysis of the psychological state of both dogs and humans [20]. Anatomically, the species-invariant rostroventral anterior cingulate cortex activity occurred in the most ventral parts of the medial prefrontal cortex and also partly in the orbitofrontal cortex, both of which have been implicated in social cognition [6]. For instance, previous imaging studies reported enhanced rostroventral anterior cingulate cortex activity when mothers saw their babies' faces [8]. Damage to the medial prefrontal cortex impairs decision-making ability [21,22]. This condition is related to a failure to cooperate with family members and society [22] and is accompanied by emotional flattening [21]. These interactions between emotion and social cognition might be subserved by the reciprocal connections between the amygdala and rostroventral anterior cingulate cortex, which could be engaged in the emotional and autonomic analysis of internal states [23]. As we used an implicit social cognition task in this study, we might be able to approach the intuitive aspects of social cognition. In addition, rostroventral anterior cingulate cortex activity was associated with emotional support from companion dogs, but not with social support from human family members. This suggests that the social cognition represented in the rostroventral anterior cingulate cortex is basic, intuitive and emotional and might underpin long-term interindividual cross-species relationships.

A previous study demonstrated greater caudal anterior cingulate cortex responses when Caucasian participants saw the faces of individuals from a different ethnic group than those from the same group [24]. This activity was significant only when the stimuli were presented for a relatively long duration, suggesting that cognitively controlled analysis was involved. These results suggest that the caudal anterior cingulate cortex is associated with the analysis of facial information according to social norms. In addition, Singer and colleagues [13] reported that caudal anterior cingulate cortex activity persisted in individuals who were subjected to painful stimuli or saw others in pain. Activation of the caudal anterior cingulate cortex is also induced by action-related judgment about humans relative to the one about dogs [14]. Taken together, these findings imply that the caudal anterior cingulate cortex is related to conspecific

cognitive analysis, which may realize complex social interactions and empathy in humans.

Conclusion

The current study has clarified the representations of species-general and species-specific social cognition. The rostroventral anterior cingulate cortex and caudal anterior cingulate cortex appear to represent different levels of social cognition. Consistent with this, Somerville and colleagues recently showed that the rostroventral anterior cingulate cortex was associated with emotional evaluation, whereas the caudal anterior cingulate cortex was related to cognitive conflicts in social acceptance/rejection judgment based on face recognition [12]. Thus, the rostroventral anterior cingulate cortex is probably associated with fundamental aspects of social cognition, which are closely related to affection. This function appears to apply to interspecies interactions without involving complex cognitive analysis. By contrast, the caudal anterior cingulate cortex might be related to higher-order social cognition, involving analyses of profit-and-loss and social norms. Thus, balancing the judgment of cognitive analysis and emotional intuition seems crucial for social interactions.

Acknowledgements

The authors thank K. Taneich and S. Tanaka for their helpful comments on the psychological testing, T. Kochiyama for support with the fMRI data analysis and D.H. Duy Thuy, N. Sawamoto and T. Murai for their critical comments on the paper. This study was partly supported by a Grant from the Companion Animal Information and Research Center (CAIRC) and also at a writing stage by a Grant-in-Aid on Fundamental Research (C) (17500210) and on Priority Areas (Mobilligence Project 17022023) from the Ministry of Education, Culture, Sports, Science, and Technology of Japan, to T.H., by a Grant-in-Aid for Scientific Research on Priority Areas System study on higher-order brain functions (18020014) from the Japan Society for the Promotion of Science, and by a grant from New Energy and Industrial Technology Development, Japan (51101244-0) to H.F.

References

1. Adolphs R. Cognitive neuroscience of human social behaviour. *Nat Rev Neurosci* 2003; 4:165–178.
2. Adolphs R. The neurobiology of social cognition. *Curr Opin Neurobiol* 2001; 11:231–239.
3. Gunter R. *Pets & people: the psychology of pet ownership*. London: Whurr Pub Ltd; 1999.
4. Hills AM. The motivational bases of attitudes toward animals. *Soc Anim J Hum-Anim Stud* 1993; 1:111–128.
5. Robinson I. *The Waltham book of human animal interaction: benefits and responsibilities of pet ownership*. New York: Pergamon; 1995.
6. Amodio DM, Frith CD. Meeting of minds: the medial frontal cortex and social cognition. *Nat Rev Neurosci* 2006; 7:268–277.
7. Leibenluft E, Gobbini MI, Harrison T, Haxby JV. Mothers' neural activation in response to pictures of their children and other children. *Biol Psychiatry* 2004; 56:225–232.
8. Bartels A, Zeki S. The neural correlates of maternal and romantic love. *Neuroimage* 2004; 21:1155–1166.
9. Nimchinsky EA, Vogt BA, Morrison JH, Hof PR. Spindle neurons of the human anterior cingulate cortex. *J Comp Neurol* 1995; 355:27–37.
10. Allman JM, Watson KK, Tetreault NA, Hakeem AY. Intuition and autism: a possible role for von economo neurons. *Trends Cogn Sci* 2005; 9:367–373.
11. Bush G, Luu P, Posner MI. Cognitive and emotional influences in anterior cingulate cortex. *Trends Cogn Sci* 2000; 4:215–222.
12. Somerville LH, Heatherton TF, Kelley WM. Anterior cingulate cortex responds differentially to expectancy violation and social rejection. *Nat Neurosci* 2006; 9:1007–1008.
13. Singer T, Seymour B, O'Doherty J, Kaube H, Dolan RJ, Frith CD. Empathy for pain involves the affective but not sensory components of pain. *Science* 2004; 303:1157–1162.
14. Mason MF, Banfield JF, Macrae CN. Thinking about actions: the neural substrates of person knowledge. *Cereb Cortex* 2004; 14:209–214.
15. Hisada M, Senda S, Miguchi M. The approaches to create a scale for students: the scale of expectancy for social support. The 30th annual meeting for the Japanese society of social psychology [in Japanese]. Tokyo: The Japanese Society of Social Psychology; 1989. pp. 143–144.
16. Taneichi K. Animal Companionship and support scale development and comparisons of scores in pet owners. The annual meeting for Japanese animal hospital association [in Japanese]. Tokyo: Japanese Animal Hospital Association; 2001. pp. 19–20.
17. Friston KJ. Statistical parametric maps in functional imaging: a general linear approach. *Hum Brain Mapping* 1995; 2:189–210.
18. Evans AC, Collins DL, Mills SR, Brown ED, Kelly RL, Peters TM. 3D statistical neuroanatomical models from 305 MRI volumes. IEEE-nuclear science symposium and medical imaging conference. San Francisco, California, USA: IEEE Services Center; 1993. pp. 1813–1817.
19. Talairach J, Tournoux P. *Co-planar stereotaxic atlas of the human brain*. New York: Thieme Medical Publishers; 1988.
20. Mitchell JP, Banaji MR, Macrae CN. General and specific contributions of the medial prefrontal cortex to knowledge about mental states. *Neuroimage* 2005; 28:757–762.
21. Damasio AR. *Descartes' error: emotion, reason, and the human brain*. New York: Avon Books; 1995.
22. Anderson SW, Bechara A, Damasio H, Tranel D, Damasio AR. Impairment of social and moral behavior related to early damage in human prefrontal cortex. *Nat Neurosci* 1999; 2:1032–1037.
23. Devinsky O, Morrell MJ, Vogt BA. Contributions of anterior cingulate cortex to behaviour. *Brain* 1995; 118 (Pt 1):279–306.
24. Cunningham WA, Johnson MK, Raye CL, Chris Gatenby J, Gore JC, Banaji MR. Separable neural components in the processing of black and white faces. *Psychol Sci* 2004; 15:806–813.

NMR IN BIOMEDICINE
NMR Biomed. 2007; 20: 743–748
Published online 8 March 2007 in Wiley InterScience
(www.interscience.wiley.com) DOI:10.1002/nbm.1139

Fractional anisotropy and mean diffusivity: comparison between 3.0-T and 1.5-T diffusion tensor imaging with parallel imaging using histogram and region of interest analysis

Yasutaka Fushimi,[1†] Yukio Miki,[1*,†] Tsutomu Okada,[1] Akira Yamamoto,[1] Nobuyuki Mori,[1] Takashi Hanakawa,[2,3] Shin-ichi Urayama,[2] Toshihiko Aso,[2] Hidenao Fukuyama,[2] Ken-ichiro Kikuta[4] and Kaori Togashi[1]

[1]Department of Diagnostic Imaging and Nuclear Medicine, Kyoto University Graduate School of Medicine, Kyoto 606-8507, Japan
[2]Human Brain Research Center, Kyoto University Graduate School of Medicine, Kyoto, 606-8507, Japan
[3]Department of Cortical Function Disorders, National Institute of Neuroscience, National Center of Neurology and Psychiatry, Kodaira, Japan
[4]Department of Neurosurgery, Kyoto University Graduate School of Medicine, Kyoto 606-8507, Japan

Received 15 August 2006; Revised 28 November 2006; Accepted 29 November 2006

ABSTRACT: We performed a comparison study focusing on differences in fractional anisotropy (FA) and mean diffusivity (MD) between 3-T and 1.5-T diffusion tensor imaging (DTI) with parallel imaging. Thirty healthy volunteers underwent DTI with an eight-channel phased-array coil at both 3 T and 1.5 T. Histogram and region of interest (ROI) analyses were performed. Paired *t* tests were applied for statistical analysis. Signal-to-noise ratios of these regions were also measured. For histogram analysis, peak location of FA was significantly lower at 3 T than at 1.5 T ($P = 0.04$). Mean FA was significantly higher at 3 T than at 1.5 T ($P = 0.002$). Peak location of MD was significantly lower at 3 T than at 1.5 T ($P < 0.001$). Mean MD was significantly lower at 3 T than at 1.5 T ($P < 0.001$). In ROI analysis, FA was significantly larger at 3 T than at 1.5 T in the centrum semiovale ($P < 0.001$), middle cerebellar peduncle ($P < 0.001$), cerebral peduncle ($P = 0.006$), posterior limb of the internal capsule ($P = 0.007$), genu ($P < 0.001$) and splenium ($P < 0.001$). FA was significantly lower at 3 T than at 1.5 T in the globus pallidus ($P < 0.001$). MD was significantly smaller at 3 T than at 1.5 T in the globus pallidus ($P = 0.007$), thalamus ($P < 0.001$), centrum semiovale ($P < 0.001$), middle cerebellar peduncle ($P < 0.001$), cerebral peduncle ($P = 0.01$), posterior limb of the internal capsule ($P < 0.001$), genu ($P = 0.01$) and splenium ($P < 0.001$). Significant differences in FA and MD exist between 3 T and 1.5 T for whole-brain histogram analysis and ROI analysis. Copyright © 2007 John Wiley & Sons, Ltd.

KEYWORDS: diffusion tensor imaging; fractional anisotropy; mean diffusivity; histogram analysis; high-field imaging; parallel imaging

INTRODUCTION

Diffusion tensor imaging (DTI) is an MRI technique sensitive to the orientation of mobility in intravoxel water molecules (1,2), and it has been widely used for studying the dependency of water proton diffusion in the brain. DTI has proven indispensable for evaluating brain structures, particularly white matter. White matter shows high anisotropy, because water diffusion is faster in the direction of fibers (3,4). *In vivo*, diffusion anisotropy in a voxel is determined by macrostructural features of the tissue, such as intravoxel fiber–tract coherence, and microstructural features of fiber density and fiber diameter (4). Degree of myelination also affects diffusion anisotropy (5).

In DTI, fractional anisotropy (FA) and mean diffusivity (MD) are two of the most commonly used scalars (6). FA decreases in isotropic water diffusion when water molecules move in all directions, and increases in anisotropic water diffusion when movement of water molecules is restricted to a specific direction. MD is equal to one-third of the diffusion tensor trace and represents a parameter of average molecular motion. FA and MD can be applied to several pathological situations in which microstructural properties of the brain are altered, such as multiple sclerosis (7–9), Alzheimer's disease (10,11) and amyotrophic lateral sclerosis (12,13). Histogram analyses offer a useful approach to whole-brain DTI analysis, as histograms can deal with whole-brain images and can be

**Correspondence to:* Y. Miki, Department of Diagnostic Imaging and Nuclear Medicine, Kyoto University Graduate School of Medicine, 54 Shogoin-Kawaharacho, Sakyo-ku, Kyoto, 606-8507, Japan.
E-mail: mikiy@kuhp.kyoto-u.ac.jp
†These authors contributed equally to the study.
Contract/grant sponsor: Health and Labour Sciences Research of Japan; *contract/grant number:* H15-003.

Abbreviations used: DTI, diffusion tensor imaging; FA, fractional anisotropy; MD, mean diffusivity; ROI, region of interest; SNR, signal-to-noise ratio.

compared among many subjects with low observer variability; in contrast, region of interest (ROI) analyses are observer dependent (14–16).

High-field MRI has become popular in clinical situations and research. Numerous reports have featured the differences in MRI at 3 T and 1.5 T, but few investigations have focused on differences in DTI (17,18). Parallel imaging using multi-channel head coils has now been introduced, and its advantages for DTI at higher fields have been reported (19). However, to the best of our knowledge, no studies have yet focused on differences in DTI with parallel imaging between 3 T and 1.5 T.

The purpose of this study was to elucidate differences in FA and MD for whole-brain images derived from DTI between 3 T and 1.5 T, using parallel imaging techniques.

MATERIALS AND METHODS

Subjects

The subjects were 30 healthy volunteers (15 men, 15 women; mean age, 28 years; range 21–46 years) with no history of neurological injury or psychiatric disease. Either a neurologist or a neurosurgeon examined each subject. None displayed any abnormal neurological signs or symptoms. Institutional review board approval was obtained for all study protocols, and all subjects provided written informed consent.

Data acquisition

All subjects underwent both 3 T and 1.5 T DTI consecutively in random order on the same day, with a whole-body 3-T MR scanner (Magnetom Trio; Siemens, Erlangen, Germany) and a 1.5 T MR scanner (Magnetom Symphony; Siemens). All underwent both 3 T and 1.5 T MRI with an interval of less than 1 h. DTI was performed using an integrated parallel acquisition technique and a receiver-only eight-channel phased-array head coil for both MR units. DTI sequences for both 3 T and 1.5 T used the same single-shot spin echo echo planar sequences. The generalized autocalibrating partially parallel acquisitions algorithm was applied with a reduction factor of 2 to shorten the *TE*: *TR*, 5200 ms; *TE*, 79 ms; field of view, 220 mm; matrix, 128 × 128; 3 mm thickness without interslice gap (matrix size, 1.7 mm × 1.7 mm × 3 mm); and four times repetition. Motion-probing gradients were applied along 12 different non-colinear directions with a b factor of 700 s/mm^2. A total of 40 slices covered the entire brain including brainstem and cerebellum. Scan time for both 3 T and 1.5 T DTI was 7 minutes 40 seconds.

DTI post-processing

MR data from DTI were transferred to a Windows PC workstation from the MR scanners. Tensor calculations were made using DtiStudio version 2.02 software (H. Jiang, S. Mori; Department of Radiology, Johns Hopkins University, Baltimore, MD, USA) (20,21). Binary brain mask images were made for diffusion-unweighted ($b = 0$) images by using SPM2 (Wellcome Department of Imaging Neuroscience, London, UK) and Matlab version 6.5 (The MathWorks, Natick, MA, USA). As FA and MD images were created from both diffusion-weighted and diffusion-unweighted images, they shared the same matrices. Skull and cerebrospinal fluid space were removed from data using the brain mask, and FA and MD images of the brain were created.

Histogram analysis

Histograms were created for each FA and MD image with a binwidth of 1% of maximum using ImageJ (National Institutes of Health, Bethesda, MD, USA), and were divided by each entire brain voxel for normalization. Peak locations, peak heights, and mean FA and MD were derived and evaluated.

ROI analysis

ROI-based analysis was also performed. The cerebral peduncle and middle cerebellar peduncle were selected as infratentorial structures, and the thalamus, globus pallidus, centrum semiovale, posterior limb of the internal capsule, and genu and splenium of the corpus callosum as supratentorial structures (Fig. 1). ROIs were placed manually on diffusion-unweighted images. Signal-to-noise ratios (SNRs) of the ROIs (middle cerebellar peduncle, globus pallidus, centrum semiovale, splenium) was calculated from the means of the ROI and standard

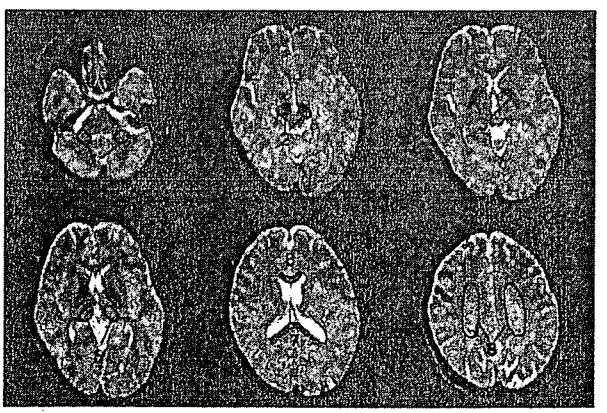

Figure 1. Diffusion-unweighted imaging ($b = 0$). The following ROIs were manually selected: 1, middle cerebellar peduncle; 2, cerebral peduncle; 3, globus pallidus; 4, posterior limb of the internal capsule; 5, thalamus; 6, genu and 7, splenium of the corpus callosum; 8, centrum semiovale